2011

Calibration of Alumina-epoxy Nanocomposites Using Piezospectroscopy for the Development of Stress-sensing Adhesives

Amanda L. Stevenson
University of Central Florida

CALIBRATION OF ALUMINA-EPOXY NANOCOMPOSITES USING PIEZOSPECTROSCOPY FOR THE DEVELOPMENT OF STRESS-SENSING ADHESIVES

by

Amanda L. Stevenson
B.S. University of Central Florida, 2008

A thesis submitted in partial fulfillment of the requirements
for the degree of Master of Science
in the Department of Mechanical, Materials and Aerospace Engineering
in the College of Engineering and Computer Science
at the University of Central Florida
Orlando, Florida

Spring Term
2011

Major Professor:
Seetha Raghavan

Abstract

A non-invasive method to quantify the stress distribution in polymer-based materials is presented through the piezospectroscopic calibration of alumina-epoxy nanocomposites. Three different alumina volume fraction nanocomposites were created and loaded under uniaxial compression in order to determine the relationship between applied stress and the frequency shift of the R-lines produced by alumina under excitation. Quantitative values for six piezospectroscopic coefficients were obtained which represent the stress-sensing property of the nanocomposites. The results were applied to an alumina-filled adhesive in a single lap shear configuration demonstrating the capability of the technique to monitor R-line peak positions with high spatial resolution and assess the stress distribution within the material prior to failure. Additionally, particle dispersion and volume fraction were confirmed with spectral intensities, introducing a novel experimental method for the assessment of quality in manufacturing of such nanocomposites. Results were further used to initiate studies in determining the load transfer to the nanoparticles and assessing the fundamental driving mechanisms.

This work is dedicated to my family whose endless support helped me get to where I am today.

Acknowledgments

I would first like to thank my advisor and Thesis Chair, Dr. Seetha Raghavan, for her extraordinary support, guidance, and encouragement throughout the entirety of this project. My sincere gratitude is offered to Dr. Raj Vaidyanathan and Dr. Ali P. Gordon for their expertise and advice, making this project a success. My personal thanks also goes to Dr. Nina Orlovskya and Dr. Raj Vaidyanathan for use of their equipment and facilities, which enabled the creation of the specimens presented in this work. Great appreciation is also given to the following University of Central Florida students for their combined assistance with sample fabrication and equipment support: Ashley Jones (Undergraduate, Mechanical Engineering), Chris Penny (Undergraduate, Mechanical Engineering), Bharathi Mohan (Graduate, Mechanical Engineering), Melan Jansz (Graduate, Mechanical Engineering), and Greg Freihofer (Graduate, Aerospace Engineering). Recognition is also given to Hong Tat, from the Boeing Corporation, for her valuable advice and support. This work was funded by the UCF ORC In House Research Grant. Use of the Center for Nanoscale Materials was supported by the U. S. Department of Energy, Office of Science, Office of Basic Energy Sciences, under Contract No. DE-AC02-06CH11357.

TABLE OF CONTENTS

LIST OF FIGURES

LIST OF TABLES

CHAPTER 1
INTRODUCTION

1.1 Motivation and Background

The ability to accurately assess integrity and predict the onset of failure in aerospace structures is complex, yet imperative for structurally sound designs and to ensure continued safety in operation. Over the last 50 years, the surge in usage of composites and corresponding bonded joints in aerospace structures has led to increased use of polymer adhesives in areas ranging from fuselage components to wing structures, as well as the joining of fiberglass composite parts [24, 68, 69, 48, 47]. This further emphasizes the need for non-invasive methods to assess the integrity and quality of adhesive joints both in laboratory testing and in operation. Many advantages stem from the use of adhesives including the elimination of stress concentrations created by typical metallic fasteners and rivets, a decrease in the overall weight of the structure, and reduced assembly times. Structural failure in bonded joints are the result of delaminations, disbonds, porosity, voids (high volume porosity), incorrect matrix cure, and cracks which alter the structure's overall load-carrying capability. In aerospace structures, various loading scenarios including static loads, vibration, and fatigue can lead to the eventual weakening and failure of these bonded joints. While ultrasonic techniques are the primary source for structural integrity monitoring of disbonds and voids, these methods are unable to assess and identify the weak bonds prior to debonding. The ability to detect weak bonds preceding failure is of significance and new and promising laser-based and thermographic

methods are currently being researched [8] to address this. Active thermography is based on differences in heat diffusion in the presence of air gaps due to voids or delamination but is limited in its ability to detect weak bonds due to low diffusion response and resolution. Laser bond inspection uses a shock wave generated by plasma originating from a high power laser with short pulse on the front surface which propagates through the inspected structure in compression and its reflection on the back surface provokes a tensile strength [2]. Such a technique is based on the principle that a weak adhesive bond would be disbonded whereas a good adhesive bond would not be damaged by a determined tensile stress induced by the shock wave [8]. However, besides being invasive in nature, such methods lack the ability to provide quantitative measurements that can relate to the integrity of a bond prior to weakening and failure.

In addition to integrity assessment, there is also a need for high spatial resolution and in-situ laboratory based techniques to advance research in adhesives with improved mechanical strength. Standard techniques for measuring stress distributions within a material, such as the use of traditional strain gauges [68], are limited in the ability to achieve high spatial resolution and are invasive in nature. They are further limited in the ability to assess load transfer mechanisms and identify localized and/or time-related initiation of failure. Research on the mechanisms of adhesive failure and effects of modifying fillers in advanced adhesives would be greatly enhanced by the ability to map the stress evolution within the adhesive towards failure in standard adhesive tests with high spatial resolution.

A novel approach which allows for the non-destructive determination of real-time stress distributions prior to failure is offered here by enabling and calibrating advanced adhesives that have stress-sensing capabilities. By embedding a polymer matrix with photo-luminescent α-alumina nanoparticles, in-situ non-invasive monitoring of stress distribution is enabled in these adhesives. A schematic of this concept is illustrated in Figure 1.1. Relating quantitative stress measurements from such a technique and the stress evolution with the weakening and failure of the bonded joint would allow for integrity monitoring. The successful development of such high spatial resolution stress-sensing capabilities in adhesives can effectively be extended to coatings that can be applied directly on structures, as well as to matrix materials in composites with the appropriate calibration.

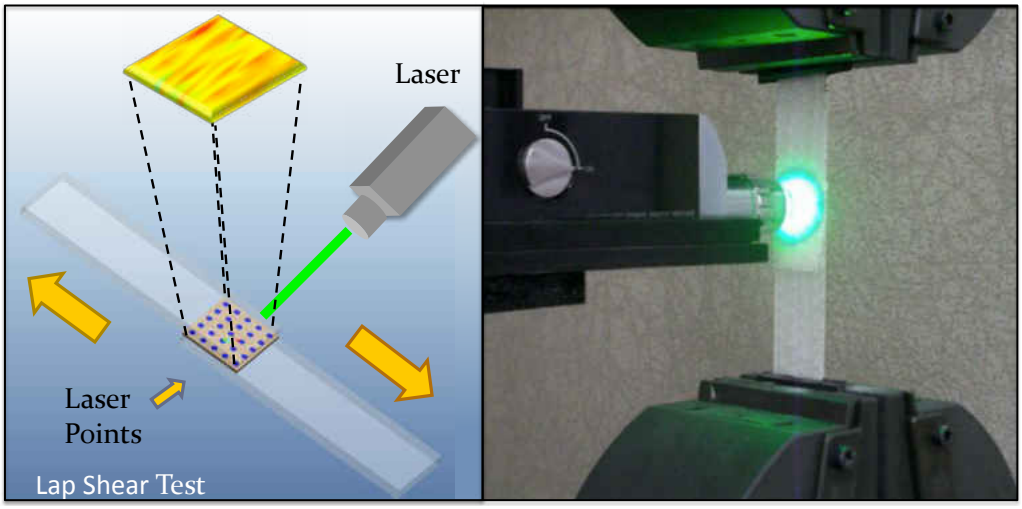

Figure 1.1: Concept for stress-sensing adhesive

1.2 Photo-Stimulated Luminescence of α-Alumina Nanoparticles for Stress Sensing

The basis of the stress-sensing capability presented here for alumina-epoxy nanocomposites is the photo-stimulated luminescence emission of chromium-doped alumina and the behavior of the emission spectra with stress. This behavior, known as the piezospectroscopic effect (PS), directly correlates stress to an observed shift in characteristic luminescence lines found in α-alumina. These spectral lines, known as the R-lines, can be identified readily as two sharp and closely spaced peaks and arise directly from chromium (Cr^{3+}) ions that naturally inhabit the crystal structure of alumina. These impurities randomly replace aluminum ions within the trigonal crystal geometry of alumina. The R-lines, illustrated in Figure 1.2, are the resulting spectral emission that occur when laser excitation causes the chromium (Cr^{3+}) ions in α-alumina to transition from an excited state back to ground state. This distinct spectrum forms the basis for the method of piezospectroscopy.

Applications using the PS technique began with the widespread use of the R1 line to monitor pressure in diamond anvil cells [1] followed by the determination of stresses in polycrystalline ceramics [32, 53, 4] and alumina-filled composites for electronic applications [45]. The method gained importance over the last two decades as a means to assess the integrity of the thermally grown oxide (TGO) layers of thermal barrier coatings [46, 15, 51, 59] on jet engine turbine blades as illustrated in Figure 1.3. These ceramic

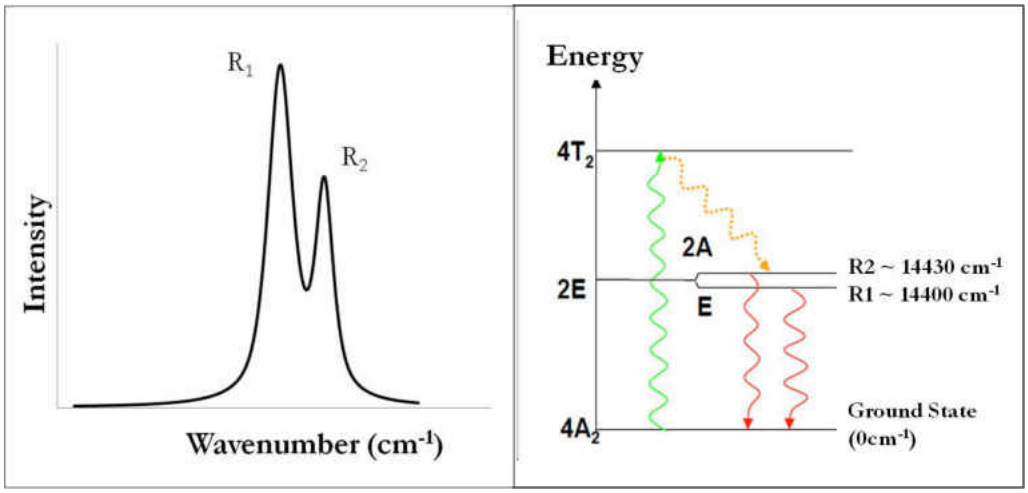

Figure 1.2: Emission spectra of Cr^{3+} ions doped in alumina.

coatings on the turbine blades enable their operation at high temperatures. They are exposed to cyclic thermo-mechanical loads which results in spallation of the coatings over time with complex stress variations in the multi-layered coating system [3]. The ability to measure the thermally grown oxide layer stress using piezospectroscopy as a function of the cycles allows for an understanding of the effects of thermo-mechanical cycling on the stresses leading to failure and contributes to life assessment studies of the coatings. The planar stress assumptions made in the existing piezospectroscopic theoretical model with 2 R-lines limits the measurement of the stress in the TGO. This has motivated efforts to extend the capabilities of this method accomplished through the measurement and the deconvolution of the less-studied vibronic band region in accompaniment with the R-lines in the emission spectra of polycrystalline alumina [52, 53].

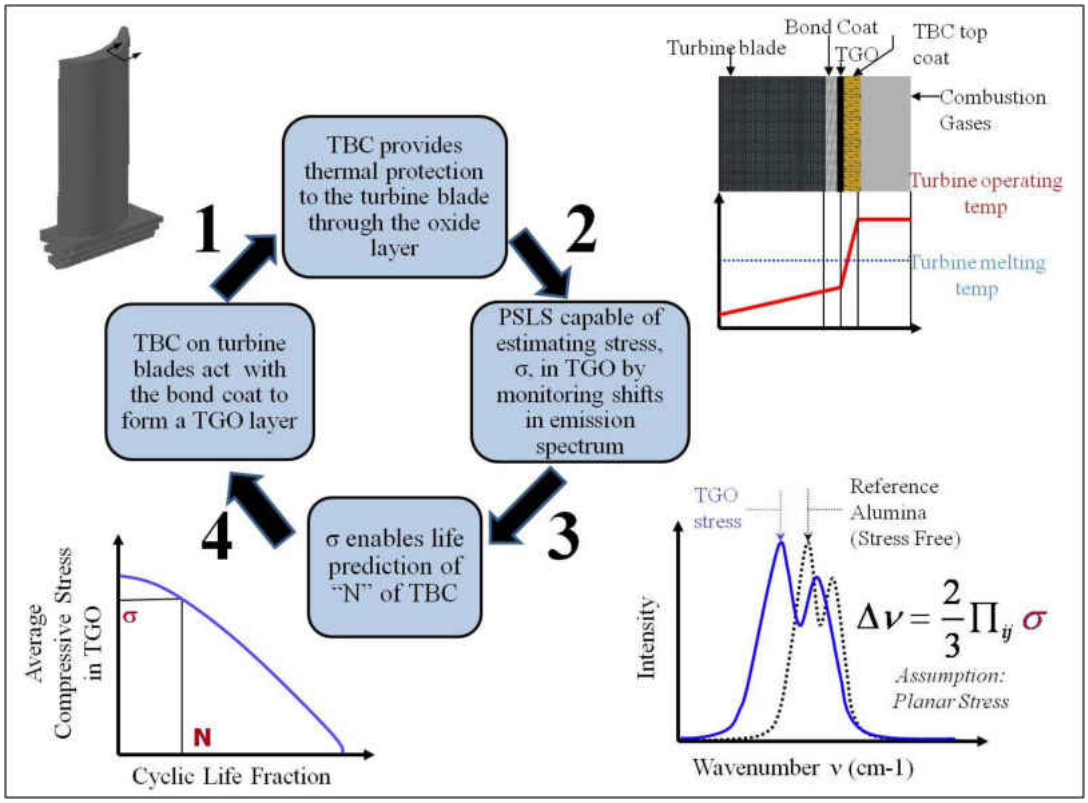

Figure 1.3: Application for PSLS technique for TBC on turbine blades

1.3 Effects of Nanoparticle Modifiers on Mechanical Properties

In the process of developing stress-sensing materials, additionally important are the mechanical properties of the particle-polymer system. Specifically, the incorporation of the modifiers cannot provide a negative impact on the mechanical properties of the composite [68]. Several studies indicating improvements in mechanical properties have been highlighted with ceramic reinforcing particles including enhanced impact properties [30, 50, 40, 58, 57, 7, 71] for lighweight armor applications. The selection of an epoxy resin as the matrix material for this work was influenced by current improve-

ments in aircraft designs that are arising due to the use of polymer adhesive bonding of primary aircraft structures. As compared to standard metals, however, unreinforced polymers have inferior mechanical properties and also exhibit poor resistance to crack initiation and propagation. Therefore, their mechanical properties must be enhanced prior to operational use. Recent efforts have already successfully shown improvements of the mechanical properties of polymer adhesives, such as increased adhesion, toughness, and peel strength [16], by reinforcing them with micron- or nano-sized particles. By doing so, the already dense cross-linked network structure of the epoxy is further increased, providing a higher strength and stiffness. Commonly used filler particles include silica [64], aluminum oxide [16, 57, 70, 63, 37] and titanium oxide [63, 10], and range from micron- to nano-sized particles. While micron-sized particles are typically more convenient to embed, the use of nano-particles ensures a higher surface-to-volume ratio [17], resulting in superior mechanical properties of the polymer matrix. A correlation between filler quantity and mechanical property improvement has been developed, indicating that there is a limit to which these particles can be added while still achieving uniform dispersion. According to Gilbert et. al. [16], an adhesive containing 10% nanoparticles by weight serves as a maximum mixture ratio, while Munson et. al. [44] identified an upper limit for nanoparticle modifiers to be 43% nanoparticles by volume. Uniform particle dispersion is essential, as this ensures an even stress distribution throughout the polymer under loading conditions. Furthermore, non-homogenous particle dispersion facilitates

agglomerations, allowing specific regions to absorb more stress than surrounding areas and creates an unbalance of the stresses.

1.4 Overview of Research

To evaluate the reliability of the mechanical properties of an adhesive or coating, it is imperative to understand the material behavior due to stress as it tends toward failure. The motivation of this work was to enable a real-time evaluation of the stress distribution within a polymer material using alumina particles as stress sensors. This will facilitate the development of new adhesives with optimal mechanical properties. Our recent work [67, 66] has shown that stresses within polymer compounds can be obtained non-destructively by infusing the material with photo-luminescent nanoparticles and measuring the observed photo-stimulated luminescence peaks as they shift due to an applied, external stress. Alpha alumina ($\alpha - Al_2O_3$) nanoparticles were specifically chosen for this study as the polymer modifier due to their capability through photoluminescence to provide a wealth of information regarding particle dispersion and stress distribution within the polymer matrix. Using epoxy composites embedded with various volume percentages of α-alumina, a calibration for optimal particle quantity was achieved non-invasively using the method of piezospectroscopy. Chapter 2 describes the theory of piezospectroscopy as it has been developed for single crystal and polycrystalline chromium-doped alumina. In this chapter, the applicability of the theory and calibration

of PS coefficients to alumina nanoparticles in an epoxy matrix is discussed. In addition, the spectral analysis procedure, which is of significance in the accurate determination of peaks positions for stress determination through deconvolution and fitting, is presented.

While the focus of this work uses alumina particles as stress sensors which are incorporated into a polymer system, the major challenges arise in the design and fabrication of the material itself. Particle dispersion quality and the quantification of satisfactory volume fraction and/or weight percentages of the filler materials are the most significant design parameters to optimize. In addition to the details of the manufacturing of the alumina-epoxy nanocomposites used in our studies, Chapter 3 highlights the experiments and studies conducted for the dispersion assessment of the samples of different volume fractions. Here, as a corollary to our research objectives, a novel method of dispersion assessment and volume fraction determination was established using the spectral intensities of the material. This method has the potential to be developed and used as a quality control tool for dispersion of similar particle-reinforced composites. In addition, this chapter describes the novel instrumentation [13] used in our studies to enable stress mapping with high spatial resolution in-situ with load.

The major focus of our work are the calibration experiments and results presented in Chapter 4. These calibration tests were performed under controlled compressive loading to obtain spectral data with increasing load. The outcomes of the calibration tests are presented as piezospectroscopic coefficients for the alumina-epoxy nanocomposite materials. The effects of the external environment, specifically the temperature, on the peak

positions is of significance to ensure that the calibrated shifts are entirely stress induced. A set of experiments assessing the effect of temperature are presented in this chapter with results indicating the negligible effect of temperature in the peak position shifts. In addition, the residual stress innately produced in the samples during manufacturing is presented and briefly discussed to highlight the variations in the different volume fraction nanocomposites. It is noted that the manufacturing induced stresses, or residual stresses, are taken as the reference or baseline condition in all piezospectroscopic studies and their significance only lies in the knowledge of a varying baseline which depends on the choice of volume fraction of alumina used for the development of such a stress-sensing material. The new results representing the PS behavior of alumina-epoxy nanocomposites presented for the first time are discussed with respect to our knowledge of the PS behavior of polycrystalline alumina. The important findings in this chapter provide quantitative information paving the way for the development of effective stress sensing materials in various applications. The significance of our measurements on load transfer studies in the area of particle reinforcement is discussed in this chapter.

An application of stress measurement in an alumina-filled epoxy adhesive under a single lap shear test is presented in Chapter 5. Currently used methods to assess adhesive integrity is discussed and compared to our proposed technique, which involves the use of embedded alumina particles as stress sensors within an epoxy matrix. Using calibrations established from the nanocomposite experiments, a single lap shear specimen with the ideal nanoparticle content was developed for optimal photo-luminescence data

collection. Contour maps described in Chapter 3 were used to observe the stress distribution throughout the adhesive with applied incremental loads. These results provide the potential for monitoring the stresses within an adhesive in a real-time environment.

Chapter 6 summarizes our findings and the implications of these findings in the development of stress-sensing adhesives using piezospectroscopy and in areas of nanocomposite development and nanoparticle reinforcement. Future directions in the use of the technique in understanding fundamental behavior of adhesives and load transfer in reinforcing particles are discussed.

CHAPTER 2
THEORY AND ANALYSIS IN PIEZOSPECTROSCOPY

2.1 Theory of Piezospectroscopy

Investigation regarding the evolution of the piezospectroscopic effect (PS) and the corresponding theoretical principles in alumina materials ($Al_2O_3Cr^{3+}$) is extensive. A shift in the characteristic R-lines of α-alumina results when the crystal field that encompasses the chromium (Cr^{3+}) ions within the alumina distorts due to applied stress causing a change in the energy of the electronic transfers cite [42, 54]. Gaining popularity as the first laser material, ruby (Cr^{3+}-doped sapphire) crystals were studied and applied to a variety of applications including the elucidation of the crystal field theory of ruby luminscence [11].

While determining the behavior of ruby absorption and luminescence spectra due to uniaxial compression, Kaplyanskii [27] subsequently introduced the first model of the PS effect, which is expressed by the following equation:

$$\Delta\nu = A(\sigma_1 + \sigma_2) + B\sigma_3 \tag{2.1}$$

where σ_1, σ_2, σ_3 are the normal stresses directed along the crystallographic axes and A and B are parameters known today as the piezospectroscopic (PS) coefficients. This equation represents the frequency shift ($\Delta\nu$) as a linear function of stress, due to symmetry.

The potential for the use of the PS effect in further applications arose due to the work by Forman [12], who first used the spectral shift of the R-lines to monitor the hydrostatic stresses in diamond anvil cells (DAC). Modifying the previous theoretical models for the PS effect, Forman developed the following relationship between the frequency shift of the R-lines and hydrostatic stress:

$$\Delta\upsilon = \pi\sigma_H \tag{2.2}$$

where σ_H is the hydrostatic stress and π represents the PS coefficient

Grabner [18] later determined the relationship between an observable shift in spectral peaks with stress and provided the following tensorial expression:

$$\Delta\nu = \pi_{ij}\sigma_{ij} \tag{2.3}$$

where $\Delta\nu$ is the frequency shift, π_{ij} represents the piezospectrocopic coefficients, and σ_{ij} is the stress state with respect to the crystallographic frame of reference. Grabner proposed that π_{ij} is symmetric, and therefore, σ_{ij}=σ_{ji}. From this, Grabner calculated the isotropic stress as:

$$\frac{1}{3}(\sigma_1 + \sigma_2 + \sigma_3) \tag{2.4}$$

In later work, He and Clarke [23] determined that point symmetry cannot be assumed, as it degenerates with applied stress. The following equation represents the updated tensorial expression after applying a coordinate transformation to a global coordinate

system:

$$\Delta\upsilon = \pi_{ij} a_{ik} a_{jl} \sigma'_{kl} \tag{2.5}$$

He and Clarke then modified the above equation to include the transformation of the frequency shift, $\Delta\upsilon$, by averaging Equation 2.5 over many randomly oriented grains. The new, reduced model for polycrystalline alumina is given by:

$$\overline{\Delta\upsilon} = \frac{1}{3}(\pi_{11} + \pi_{22} + \pi_{33})(\sigma_{11} + \sigma_{22} + \sigma_{33}) \tag{2.6}$$

This model could be further reduced by neglecting tranverse stress ($\sigma_{33} = 0$) and assuming equal in plane stresses ($\sigma_{11} = \sigma_{22} = \sigma$):

$$\overline{\Delta\upsilon} = \frac{2}{3}(\pi_{11} + \pi_{22} + \pi_{33})\sigma \tag{2.7}$$

He and Clarke's work in determining the coefficients of the PS tensor for ruby gave the following expressions for the frequency shift of the R-lines in terms of the three crystallographic directions:

$$\Delta\nu\,(R_1) = 2.56\sigma_{11} + 3.50\sigma_{22} + 1.53\sigma_{33} \tag{2.8}$$

$$\Delta\nu\,(R_2) = 2.66\sigma_{11} + 2.80\sigma_{22} + 2.16\sigma_{33} \tag{2.9}$$

The PS coefficients were determined by observing the frequency shift corresponding to uniaxial compression along the three principal crystallographic axes. In later work, He and Clarke expanded upon their PS effect models by evaluating the room temperature polarization characteristics of ruby R-lines. The consequences of the polarization on

piezospectroscopic measurements are presented below [22, 35, 34, 14]:

$$\Delta\nu_{R1} = 3.26(\sigma_{11} + \sigma_{22}\cos\theta^2 + \sigma_{33}\sin\theta^2) + 1.53(\sigma_{22}\sin\theta^2 + \sigma_{33}\cos\theta^2) \tag{2.10}$$

$$\Delta\nu_{R2} = 2.73(\sigma_{11} + \sigma_{22}\cos\theta^2 + \sigma_{33}\sin\theta^2) + 2.16(\sigma_{22}\sin\theta^2 + \sigma_{33}\cos\theta^2) \tag{2.11}$$

The study of the vibronic sidebands in the emission spectrum by Raghavan and Imbrie [53, 51] revealed multiple peaks within these bands to exhibit stress-sensitive behavior indicating the potential for extending the piezospectrocopic model.

Building on the theoretical basis for the PS effect for a polycrystalline material, when considering our case in which alumina particles are embedded within a polymer matrix, the PS coefficient can be directly related to the applied stress and frequency shift of the R-lines using the following expression:

$$\Delta\nu_{NC} = \Pi_{NC}\sigma_{applied} \tag{2.12}$$

where $\Delta\nu_{NC}$ is the frequency shift of the alumina R-lines embedded in the nanocomposite, Π is the PS coefficient, and $\sigma_{applied}$ is the stress applied to the nanocomposite.

2.2 Deconvolution and Curve Fitting

To properly study stress effects using piezospectroscopy, the deconvolution and fitting of the α- alumina produced R-lines is crucial to ensure accurate and precise peak positions throughout the entire procedure. Unfortunately, these values are not readily available

from the experimental data as the R-lines share data due to their close proximity to each other, as shown in Figure 1.2.

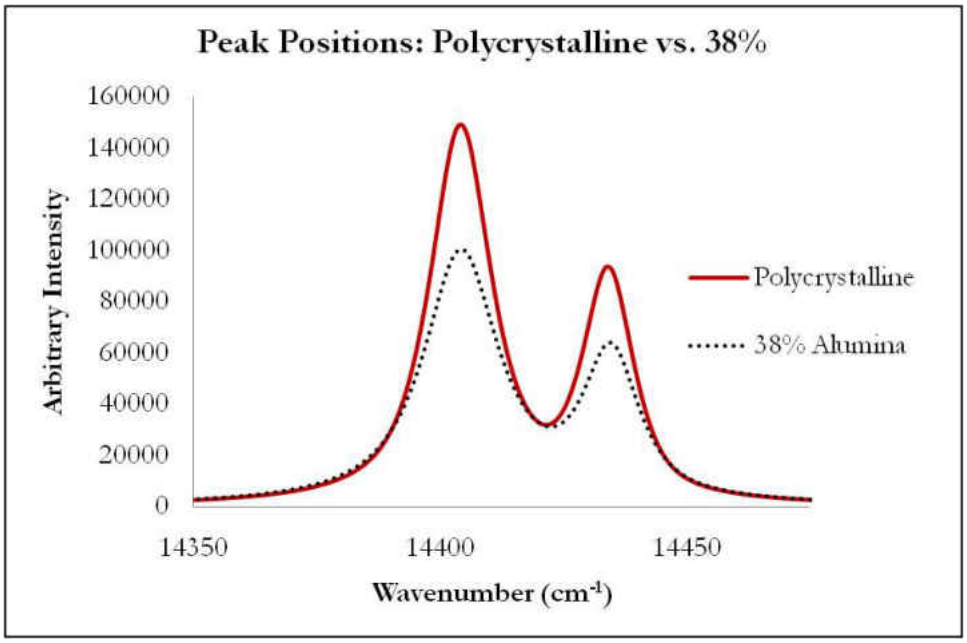

Figure 2.1: R-lines obtained from polycrystalline alumina and the 38% nanocomposite. The overall shape distribution of the curves is similar.

This overlapping region affects the exact position of the curves, making it necessary to process the raw data using a curve-fitting technique that generates the correct peak positions. Throughout this work, a genetic algorithm (GA) based procedure previously created and used to predict the correct R-line and vibronic sideband peak positions of polycrystalline alumina [52] was implemented on the unprocessed, experimental data. This GA method was preferred over gradient-based methods, as it has the capability of global optimization [65, 5]. This Matlab-based, GA method performs four main functions to optimize the R-lines: baseline removal, cropping, separation, and recombination. The

fitting procedure used two pseudo-Voigt functions [28, 62, 25] to obtain the following design variables for each of the R1 and R2 curves: area, line-widths, peak positions, and shape factors (describing the Gaussian and Lorentzian characteristics) [55]. Figure 2.2 shows the deconvolution of the R-lines.

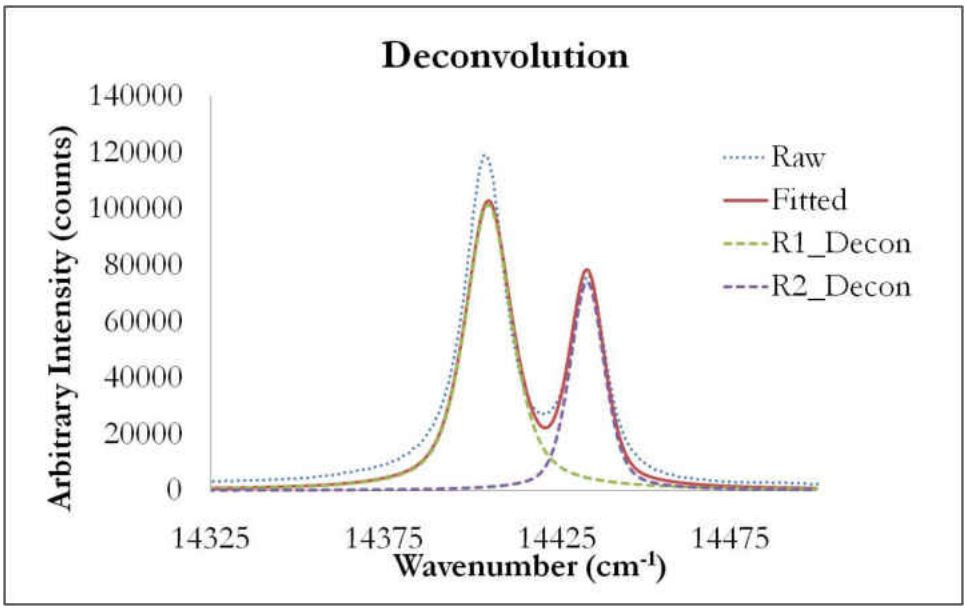

Figure 2.2: The deconvolution and fitting results for the R-lines of alumina-epoxy containing 38% α-alumina by volume.

CHAPTER 3
VOLUME FRACTION AND DISPERSION USING PHOTO-STIMULATED LUMINESCENCE INTENSITY MAPPING

3.1 Objectives

Calibrating stress-sensing alumina-epoxy nanocomposites requires the challenging task of designing and fabricating such a composite, while achieving an improvement in the overall mechanical properties of the material. Important objectives of the work presented in this chapter include verifying that sufficient luminescence intensities could be obtained from the alumina nanoparticles for spectral peaks to be monitored with stress during calibration, as well as to ensure uniform particle dispersion. Additionally, an accurate control of the volume fraction or weight percentages of the fillers was to be achieved during manufacturing of the calibration specimens. The fabrication of the samples are presented here, followed by the experimental equipment and data collection method used to assess the spectral data from different alumina volume fraction samples. The results of photo-stimulated luminescence spectra are presented for the nanocomposites and compared with polycrystalline alumina. The theory on photo-luminescence emission intensities are discussed and related to findings of the intensities from varying volume fractions. ***In achieving our objectives, a novel method to verify homogeneous particle dispersion, as well as to calibrate and identify particle volume fractions within a polymer matrix was established and implemented on the specimens investigated in this work***. Here, the photo-stimulated luminescence intensities and

integrated intensities (area under the emission spectra) from embedded α-alumina particles within polymer matrices are used as indicators of dispersion over the mapped surface. This method is applicable as a means of ensuring uniform dispersion of modifying fillers in various nanocomposites with a spectral signature and can be implemented as a quality control tool in the manufacturing of these materials. The benefits of such a non-invasive tool over conventional microscopy techniques is the high spatial resolution over a large area that can be achieved with no sample preparation requirements.

3.2 Fabrication of Alumina-Epoxy Nanocomposites of Varying Volume Fraction

Three separate composite samples were created as calibration specimens consisting of 5%, 25% and 38% α-alumina by volume. This range was established based on literature showing that a minimum of 5% volume fraction has a positive influence on mechanical properties [6] and 43% has been determined to be the maximum amount of alumina that can be added conveniently to an epoxy without having a negative effect on the overall properties of the epoxy [16]. The filler material used for this study was α-alumina nanopowder, having an average particle size of 150nm and 99.85% purity, obtained from Advanced Materials. The epoxy resin was Epon 862 which was coupled with the curing agent Epikure W, both of which were received from Hexion. The manufacturing procedure was based on literature describing the addition of alumina fillers in epoxy composites

for mechanical property improvements [50, 58, 30, 40]. For each volume fraction composite fabrication, the epoxy resin, curing agent and α-alumina particles were initially mixed using a high shear mixer for the duration of 15 minutes to break up any agglomerates present, while also dispersing the alumina homogeneously within the epoxy. Once combined, the material was then placed into a sonicator for approximately 20 minutes to further ensure homogeneity, as well as cause any entrapped air bubbles to surface for removal. The composite was then placed inside a low-pressure desiccator-vacuum system for approximately 45 minutes, or until no air bubbles were visible. The sample was then collected and poured into an aluminum mold with the dimensions 10in x 6in x 3.5in, which was first prepared with Partall Hi-Temp Wax, used as a mold release. A two-step curing process, with a duration of 6 hours at 54°C and 16 hours at 93°C, was then implemented and the specimens were allowed to cool.

3.3 In-Situ Optical Probe for Spectral Surface Mapping

A unique system consisting of an MTS Insight electromechanical testing system, fiber optic probe, XYZ stage, and Raman spectrometer was utilized in order to collect fluorescence data as tensile and/or compression loads are applied to a specimen and is shown in Figure 3.1. The Raman spectrometer was coupled with a green, argon laser which operated at a wavelength of 532 nm and exerted a maximum output power of 50 mW. The laser beam had the capability of either being directed to an attached microscope or

to a connecting fiber optic probe. The fiber optic probe was coupled with the Raman system via optical cables and worked with multiple objectives. A special mount to hold the probe stationary was created and attached to the Y-axis of the XYZ stage, while the XYZ stage itself was fastened to a platform that was built and affixed to the base of the MTS machine. The electromechanical testing system used was capable of both tensile and compression loads of up to 50 kN and was operated via the software, TestWorks 4. The operating software for the Raman spectrometer and the XYZ stage were WIRE 3.1 and COSMOS 3.1.6, respectively. This unique system [13] enabled specific regions on the surface to be mapped with a spatial resolution of about 1-2 microns.

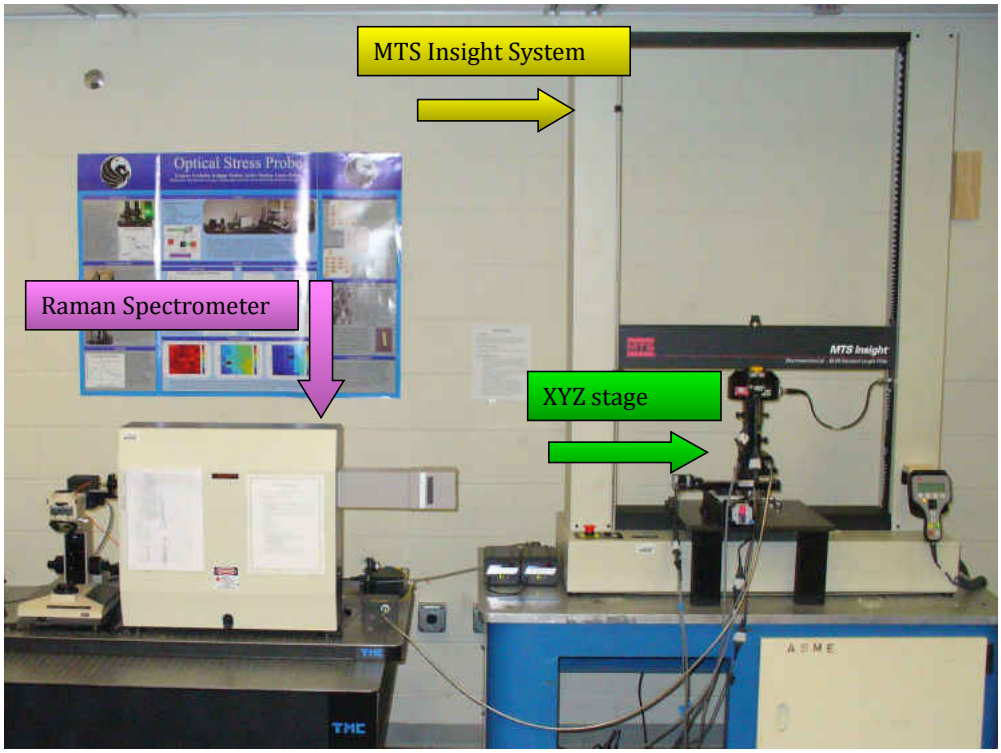

Figure 3.1: Experimental equipment setup

By focusing the optical probe on the sample surface, spectral data could be collected from several regions over the surface. The spectral data can then be represented as contour plots, created by a program written using MATLAB. When considering the intensity and integrated intensity, uneven intensities are represented by variations in the contour plots indicating a change in the amount of alumina present over the sample due to the direct relationship between luminescence emission and particle content. A variation in the contour plots when analyzing R-line peak positions represents a shift in the peaks, which is correlated to a change in the stress of the material through calibration. Therefore, using this technique, a visual inspection of homogeneity as well as stress distribution with applied stress can be obtained.

3.4 Photo-Stimulated Luminescence Spectra Obtained from Alumina-Filled Epoxy Nanocomposites

The first notable result obtained from this work is the capability of detecting and measuring the R-lines from α-alumina nanoparticles embedded within an epoxy resin. Photo-stimulated luminescence readings from all three α-alumina-epoxy nanocomposites were obtained as shown in Figure 3.2 with strong emissions from 25% and 38% samples. Additionally, a comparison of measured R-lines from polycrystalline alumina and alumina nanopowder indicates that the overall lineshape distribution between the two materials is similar, as presented in Figure 3.3. Another notable feature from this data is an evident

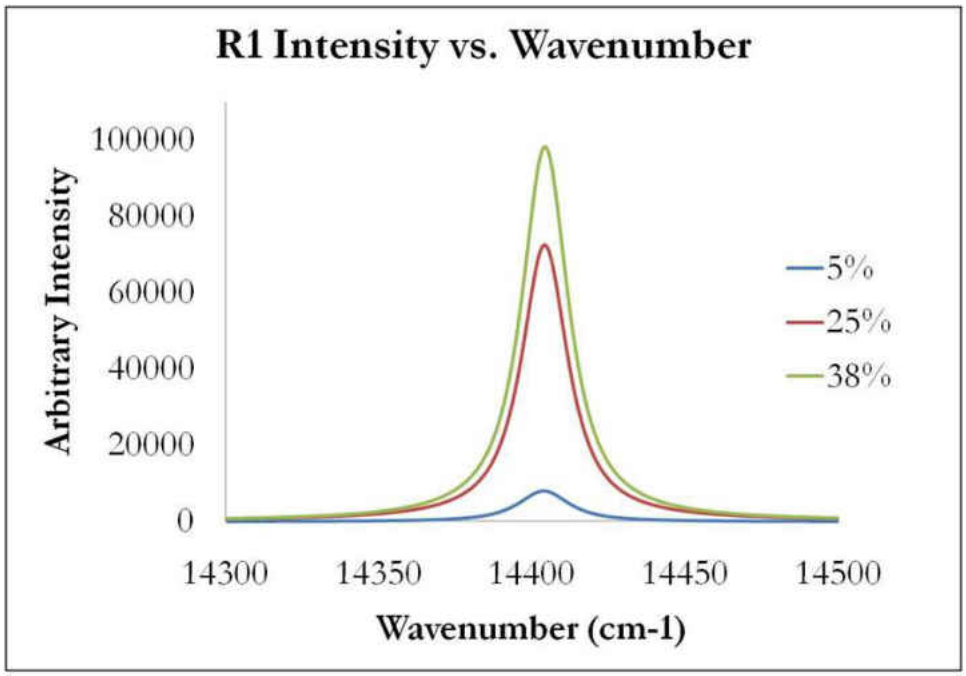

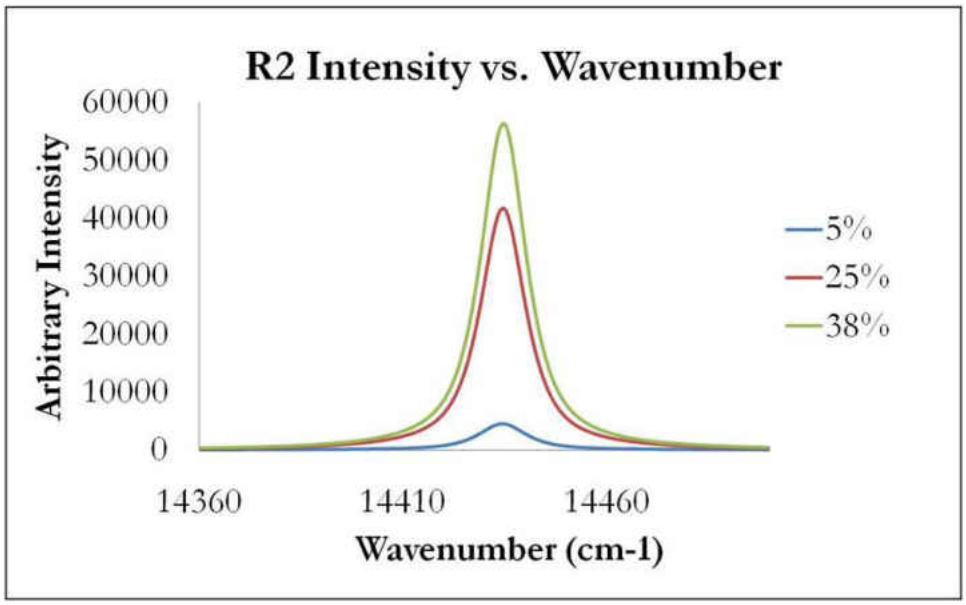

Figure 3.2: Intensities of R-lines for 5%, 25% and 38% volume fraction alumina epoxy composites

correlation between intensity and α-alumina particle quantity. It was observed that the increase in particle volume fraction was accompanied by an increase in the magnitude of the emission intensity. This phenomenon can be explained using the concept of the photon energy released due to the electronic transfers of the chromium ion from an excited state back to ground state to produce the R-lines:

$$E = h\nu \tag{3.1}$$

where E is the energy of the photon (J), h is Planck's constant,$(6.63x10^{-34}Js)$, and ν is frequency (Hz or s^{-1}).

As the concentration of α-alumina increases, the probability of the incident beam interacting with a nanoparticle also increases and is governed by the following equation:

$$P = N\sigma \tag{3.2}$$

where P is the interaction probability, N is the number of atoms or ions, and σ is the microscopic cross-section. Thus, the overall energy emitted from an α-alumina composite is directly related to the amount of photo-luminescent particles present.

By incorporating Beer's Law, the luminescence of each nanocomposite can be analyzed, predicting that there exists a relationship between absorbance (and therefore emittance) and the concentration of the material, as described by the following equation:

$$A = -\log T = -\log(\Phi/\Phi_a) = abc \tag{3.3}$$

where A is the absorbance of the material, T is the transmittance, a is the absorptivity, b is the path length of the absorption, and c is the concentration of the material that has the absorption properties

As previously mentioned, the nanocomposites configured in this study consisted only of epoxy resin and α-alumina nanoparticles. Only the chromium within the alumina exhibited luminescent properties while the other materials (the resin matrix) were optically transparent. Therefore, the measured luminescence from the specimens only describes the behavior of the chromium-doped alumina particles. It can be stated that the radiant power that is luminesced is proportional to the amount of power that is absorbed,

$$\Phi_L = k(\Phi_0 \Phi) \tag{3.4}$$

where Φ_0 is the radiant power of the incident beam, Φ is the total power transmitted, and k describes the efficiency at which an excited atom or molecule emits a photon when returning to ground state and varies by material.

Combining Beer's Law with Equation 3.4 provides the total power transmitted from a photo-luminescent material:

$$\Phi_L = k\Phi_0(1 - 10^{-abc}) \tag{3.5}$$

The ability to capture the photo-luminescence of these nanoparticles is altered, however, once embedded within a material of specified density. While the behavior of the photoluminescence of the chromium atoms is still governed by Equation 3.3, the number

of photons collected may be less than the actual number of photons emitted, due to absorbance and scattering that occurs within the material itself. Photons capable of being collected by a charged coupling device (CCD) exit the specimen in a direction parallel and opposite to the incident beam. Scattered photons will exit in various directions and are, therefore, unaccounted for in the measurement. Additionally, an emitted photon may also be absorbed by a material, prohibiting the energy from escaping.

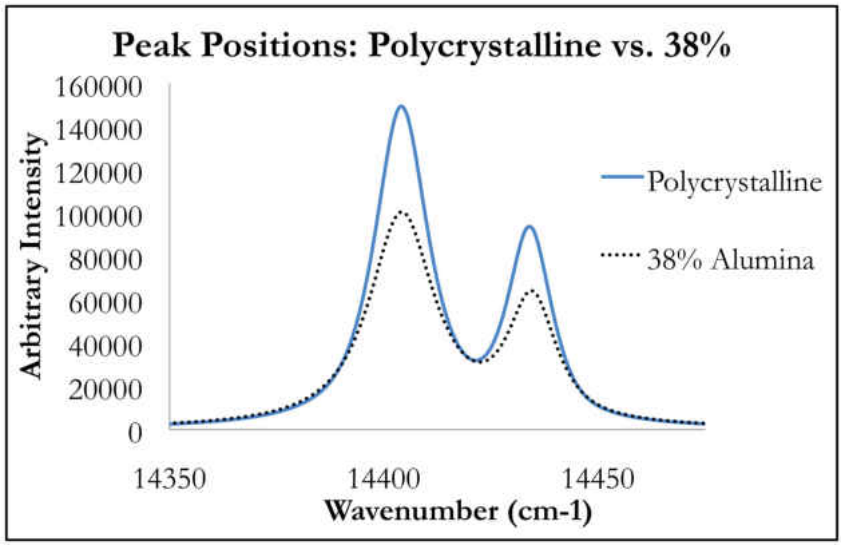

Figure 3.3: Intensities of R-lines for 38% volume fraction alumina epoxy composite compared with polycrystalline alumina

In addition, an increase in PSLS intensity resulted from the increase of alumina nanoparticles present. This relationship is shown in Figure 3.4 and may provide a potential means to establish homogeneity and/or alumina content within a specimen. If a specific photo-luminescent intensity is measured, a prediction of how much alumina is contributing to that value may be deduced by comparing it to the intensities of known

volume fraction alumina-epoxy samples. Homogeneity could be validated if the intensity at each point in the composite is the same.

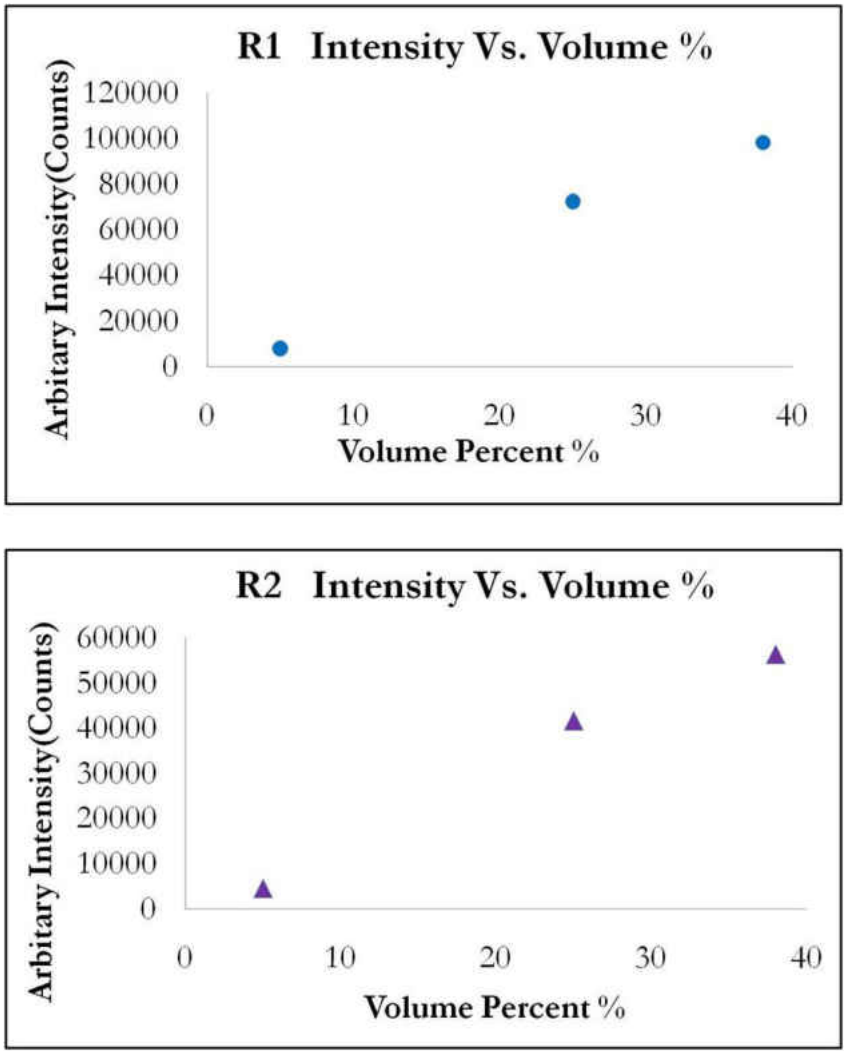

Figure 3.4: Intensities of R-lines for 5%, 25% and 38% volume fraction nanocomposites

3.5 Volume Fraction and Dispersion Results

To ascertain consistent properties throughout the sample, the composite must have a homogeneous dispersion of particles as well as be free of all inclusions, agglomerates, and aggregates, as they can contribute to stress concentrations and lead to premature structure failure. Air bubbles, voids, and any other non-composite material are deemed inclusions, while agglomerates and aggregates are essentially clumps of particles. Agglomerates can often be dissipated by high shear mixing, whereas aggregates are formed from covalent bonds and cannot be separated. Current methods for determining uniform particle distribution include the visual inspection of Scanning Electron Microscopy (SEM) and Transmission Electron Microscopy (TEM) images with the assumption that they represent the entire behavior of the specimen. Ensuring that the desired amount of modifier is added to the matrix is also an important aspect of the design process. The amount of filler particle directly affects the mechanical properties of a specimen, as it determines the cross-link density of the matrix. A composite which contains a high amount of filler particles may experience an undesirable brittle behavior, whereas one with too few particles, may not exhibit the material strength required for a specific application. By collecting data over the entire specimen surface, maps comprised of spectral characteristics can be obtained. Specifically, there are three main spectral attributes that can be analyzed: integrated intensity (area under the curve), intensity, and peak position. Through the utilization of α-alumina and its unique spectrum, these properties are col-

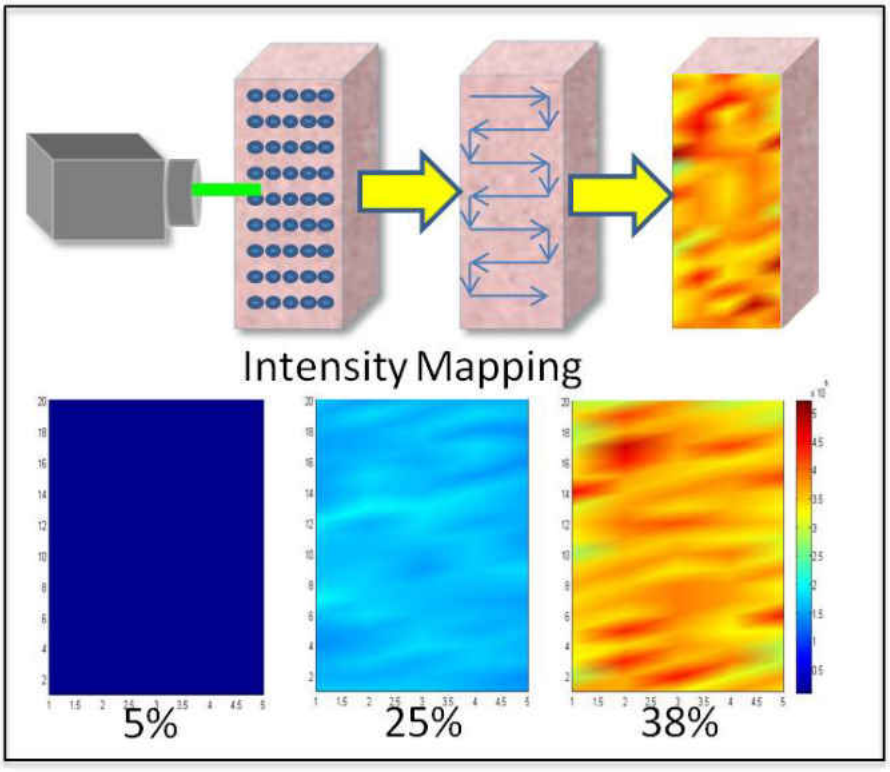

Figure 3.5: Spectral intensity mapping technique using photo-luminescence (above) and the results for our different volume fraction specimens indicating particle dispersion over the specimen surface

lected at specified surface regions and compared. The results are then visually shown via contour plots. The resolution of these surface maps is dependent upon both the number of spectral collection points taken and the objective magnification used. To date, this new method currently applies to specimens having flat surfaces, such as a prism or parallelpiped, as these are the ideal geometric shapes for fluorescent data collection. A perpendicular alignment of the surface to the excitation source is required to obtain accurate spectral results. The aim of this work is to validate the even dispersion of embedded

α-alumina nanoparticles within an epoxy resin by generating spectral surface maps using the integrated intensity characteristic. Contour maps capable of visually displaying the differences in integrated intensity throughout the sample surface were created and used to identify particle distribution, as well as locate undesirable features such as voids, agglomerations, and inclusions.

CHAPTER 4
CALIBRATION OF ALUMINA-FILLED EPOXY NANOCOMPOSITES USING PIEZOSPECTROSCOPY

4.1 Objectives

In order to calibrate alumina-epoxy nanocomposites as a stress-sensing material, we must first investigate the behavior of the photo-luminescent information received from the α-alumina nanoparticles as they are allowed to interact with the matrix material under loading conditions for various configurations of particle-matrix ratio (volume fraction). These results will be compared and verified against previous work done using polycrystalline alumina. Calibration experiments using alumina-filled epoxy nanocomposites were devised to determine the spectral peak shifts with stress or piezospectroscopic (PS) coefficients, as well as to provide a standardization between the observed PS coefficients and volume fraction. This information on the PS behavior, when coupled with mechanical property analysis, can be used for the development of optimized stress-sensing adhesives and/or coatings. These calibration experiments and results are described in the following section.

The unloaded peak positions form the baseline for the calibration experiments and all PS coefficients are taken with reference to their corresponding baseline as they are loaded incrementally. Hence, any initial residual stress in the material from the manufacturing process correlates to the zero applied load peak position and consequently does not affect

the determination of the PS coefficients. However, the differences in the zero applied load peak positions between the various volume fraction specimens provides some interesting information on the difference in residual stress due to the manufacturing process when varying amounts of alumina nanoparticles are incorporated into an epoxy matrix. This is discussed briefly in the following section.

Finally, while spectral peak shifts are known to occur with stress, existing literature indicate that external factors such as temperature also affects the peak positions. Therefore, the effect of temperature changes on the peak positions must be ascertained to establish the range of error in the PS coefficients with respect to variations in ambient temperature during the calibration process. Thermal experiments were conducted to address this and also to quantitatively establish the peak position shifts over a temperature range that the samples are exposed to. The results are presented in this chapter.

4.2 Piezospectroscopic Calibration Experiments

The alumina-filled epoxy nanocomposites used in this work were cut from bulk samples fabricated using methods previously described in Chapter 3. Three samples of each volume fraction were manufactured into parallelepipeds having a 4:1 ratio per ASTM D695. This ratio was chosen to avoid edge effects, caused by the friction between the sample surface and the platen during loading experiments which were previously observed in ex-situ studies of compression tests on polycrystalline alumina of a lower aspect ratio.

The final dimension sizes of the samples included a 1/8 in x 1/8 in cross-section and a length of 1/2 in, shown in Figure 4.1.

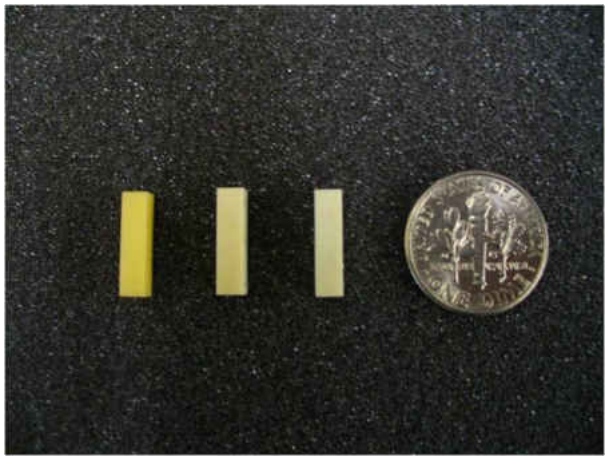

Figure 4.1: Manufactured alumina-epoxy nanocomposites consisting of different three different volume percentages of alumina, 5% (left), 25% (middle), and 38% (right)

4.2.1 Experimental Setup for PS calibration

To collect and analyze the excited fluorescence during the in-situ compression loading experiments, the experimental set-up and method presented in Chapter 2 was implemented. An argon laser operating at a wavelength of 532 nm served as the excitation source. To initialize the experiments, the laser beam was first focused on the 5% volume fraction specimen surface, using the intensity of the R1 as a calibration tool. Containing the least amount of alumina particles, the intensity received from the 5% specimen was the most important to optimize. The XYZ stage/ laser was moved incrementally backward or forward in a step size of approximately 544 microns until the R1 curve

achieved maximum intensity, indicating that the beam was now focused. This position was fixed and used as the focus position for all experiments, as the relative intensities for the 25% and 38% percent samples would be sufficient due to an increase in alumina particle quantity. For each experiment, the laser beam was initially set to the left-center of the surface. This position, along with the previously determined focusing distance, was set as the reference location, allowing for the program to return to that exact spot throughout the testing. Starting from the left-center position, individual spectra from 5 different collection points on the surface of each sample were collected in a horizontal line, as shown in Figure. The step size between each collection location was approximately 544 microns. Photo-luminescence data was captured from each position using 1 second collection intervals at 100% laser power (50mW). Per position, 50 acquisitions were obtained for statistical and averaging purposes. A neutral density filter of 40% transmissibility was used to reduce the laser power provided to 38% specimen, to allow for constant experimental parameters to be used without saturation of the charged couple device (CCD).

Each of the three manufactured α-alumina volume fraction specimens were subjected to incremental, compression loads, while photo-luminescent data was simultaneously collected. An Insight MTS electromechanical loading system applied the compressive load via steel platens. Due to the hardness of alumina, additional sapphire platens served to avoid direct contact of the sample with the platens. To ensure that the applied load was directed uniaxially throughout the specimen, plexiglass templates were specially designed

to align the sapphire platens and composites with the exact center of the compression platens. Incremental loads of 0.04 kN were applied and held for 15 minutes each while the PSLS information was obtained. The load range applied to each volume fraction sample was dependant upon the mechanical strength of each sample which was established during separate load range experiments. These experiments were run on additional samples that were compressively loaded to failure to establish the maximum loads that could be applied to each volume fraction sample before failure occurs. Table 4.2 provides the maximum load values for each of the different volume fraction specimens. All measurements were performed at room temperature.

Table 4.1: Maximum Loads and Corresponding Stress.

Volume Percent of Specimen	Maximum Load (kN)	Maximum Stress (GPa)
5	1	0.099
25	1.2	0.119
38	1.4	0.139

4.2.2 PS Coefficients Results and Discussion

Shifts in the R-lines were observed with increasing compressive load on each of the volume fraction nanocomposites. These R1 and R2 line peak shifts due to applied uniaxial compressive stress are presented individually for the 5%, 25%, and 38% volume fraction specimens in Figures 4.3, 4.4 and 4.5 respectively.

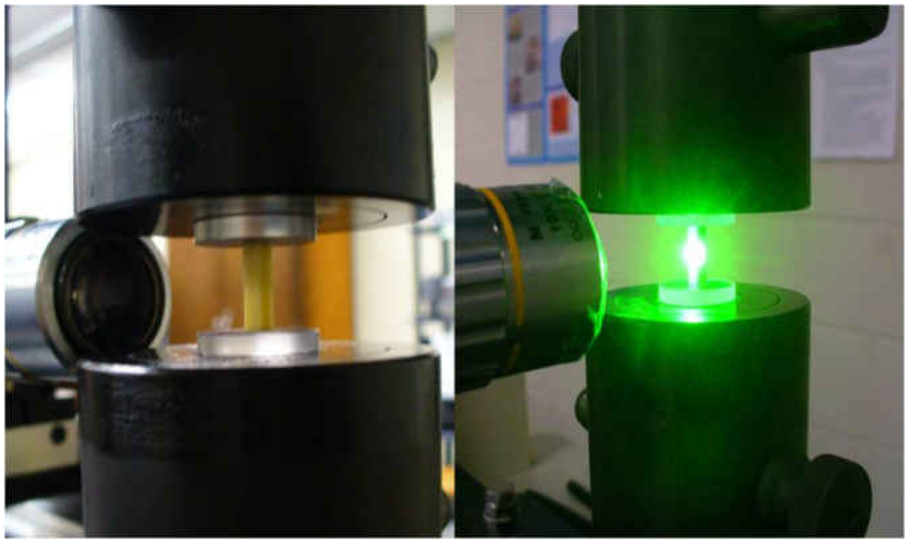

Figure 4.2: Alumina-epoxy nanocomposites under compression load

The PS coefficients corresponding to each nanocomposite material were determined as the slopes established by the collected in-situ PSLS data in these plots. The data obtained from the spectral lines indicate a linear relationship between the peak shift and applied stress with the values of the R1 and R2 PS coefficients exhibiting similar order of magnitudes to that of single and polycrystalline alumina. This linear slope is the expected piezospectroscopic behavior of the α-alumina material.

A comparison of PS coefficients to nanoparticle volume fraction are presented in Table 4.2. The results indicate that the magnitude of the R1 and R2 PS coefficients exhibit an increasing trend with the quantity of filler material (volume fraction) present. This phenomenon can be justified by analyzing the effects of mechanical properties due to

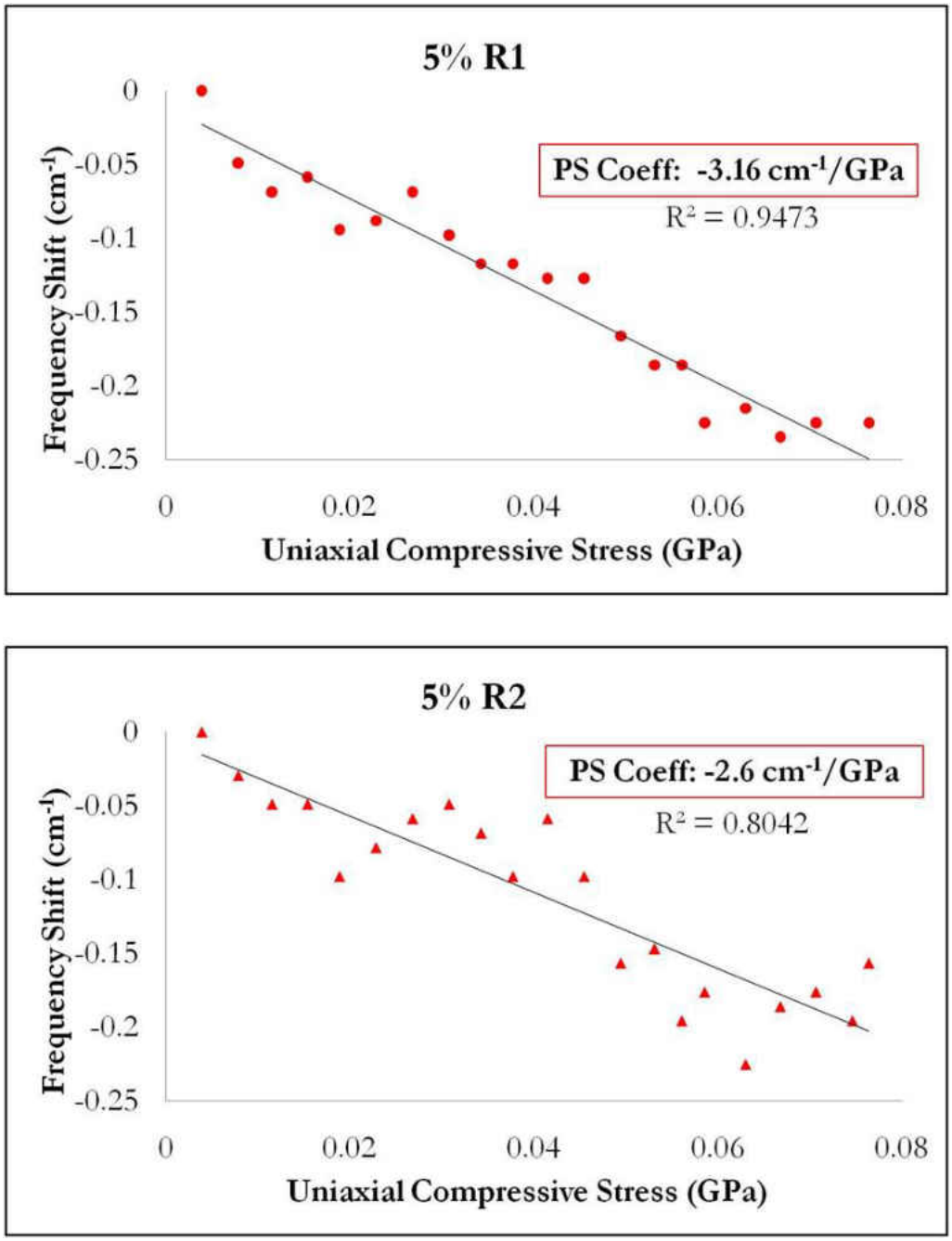

Figure 4.3: Frequency shift of the R-lines vs. stress for the 5% specimen

increased modifier content within an epoxy. Generally, a larger PS coefficient (slope) represents a larger peak shift for a given applied stress value. Since the peak shifts cor-

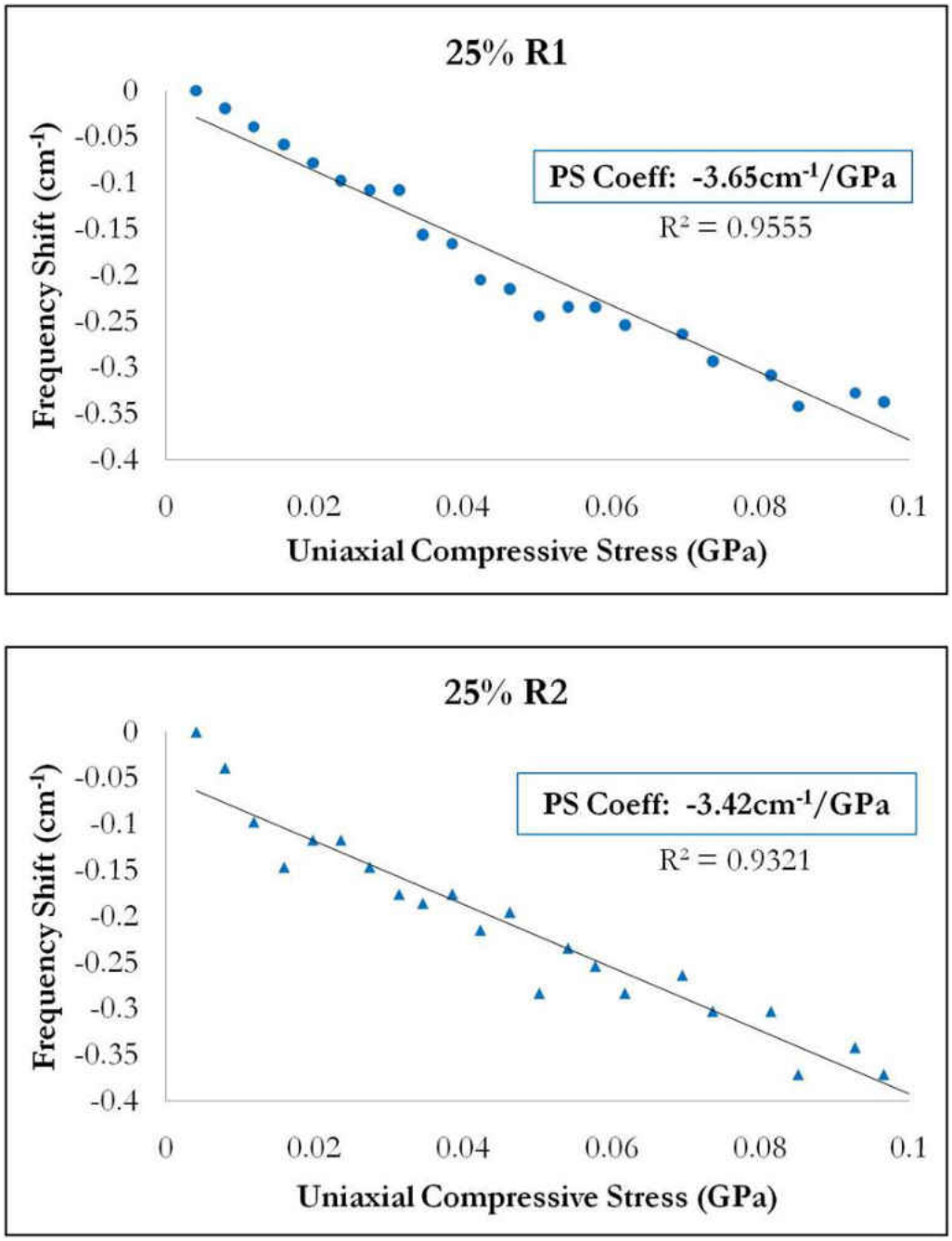

Figure 4.4: Frequency shift of the R-lines vs. stress for the 25% specimen

relate directly to the stress experienced by the α-alumina material, the nanoparticles experiencing higher stress exhibit larger R-line peak position shifts. This would indicate

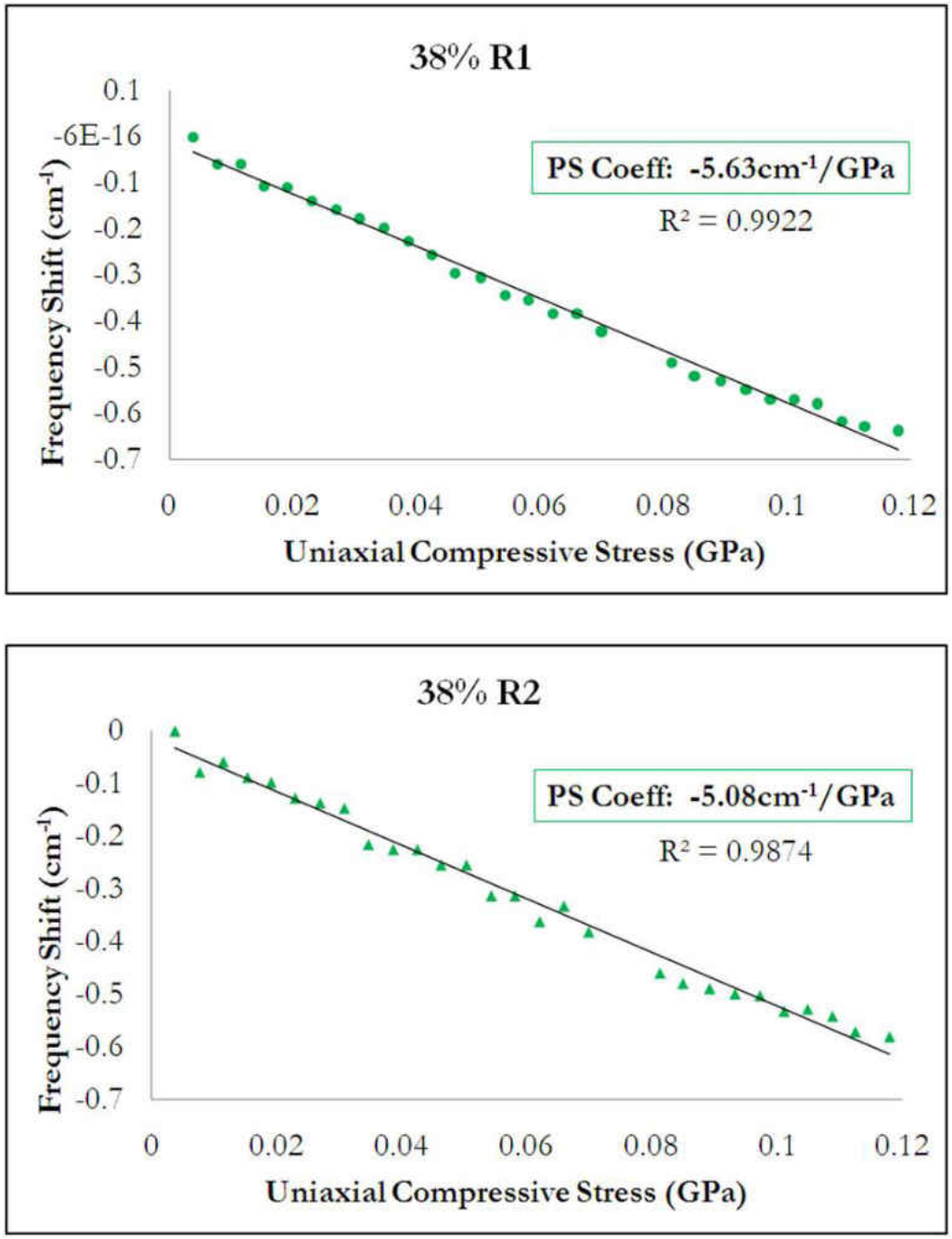

Figure 4.5: Frequency shift of the R-lines vs. stress for the 38% specimen

then, that the alumina particles contained in the 38% volume specimen are subjected to higher stresses as compared to the 5% and 25% volume composites. This can be explained

Table 4.2: R-line PS coefficients comparison (magnitude) per volume fraction specimen.

Specimen Type (Volume Percent)	R1 PS Coefficient (cm^{-1}/GPa)	R2 PS Coefficient (cm^{-1}/GPa)
5	3.16	2.60
25	3.65	3.42
38	5.63	5.08

by observing that the alumina material has a higher mechanical strength than the epoxy and is, therefore, capable of accepting more of the applied stress given to the composite. Thus,within the nanocomposites of increased volume fraction of alumina nanoparticles, a higher proportion of the applied stresses are experienced by the nanoparticles and consequently these samples can sustain higher stress before failure. This corresponds to previous experimental work verifying that specimens with a greater volume of modifier particles possess higher mechanical properties [16]. The experimental results are consistent with the theory of the rule of mixtures which defines the elastic modulus of a composite as

$$E_{NC} = v_f E_f + v_m E_m \tag{4.1}$$

where E is the elastic modulus, v is the volume fraction, and the subscripts f and m refer to the filler and matrix respectively.

Table 4.3: Elastic modulus of each volume fraction composite (E_{NC})

Volume Percent of Filler	Volume Percent of Matrix	E_{NC} (GPa)
5	95	19.9-23.1
25	75	88.3-104.3
38	57	149.9-177.4

.

The mechanical reinforcement of fillers has been studied in a variety of analysis and simulation studies with varying ideas on the load transfer mechanisms. Both particle-to-polymer interface and interparticle contact have been identified as contributors to reinforcement in polymer based nanocomposites [41]. It has been predicted that at high loads reinforcement occurs due to "particle jamming," while the particle-polymer network is of significance in low loadings [49]. These two effects are illustrated in a schematic as applied to our nanocomposites in Figure 4.6. Two main theories can be used for comparison with the measured stress in the nanoparticles with applied load. Theoretical mechanics indicate that the surface and interface elasticities are critical at the nanoscale. The governing classical Eshelby theory [9, 56] on the elasticity of an ellipsoidal inclusion was modified by taking into account corrections for a finite matrix by Gurtin et al. [20]. Recently, Mi et al. [39, 38] solved the axisymmetric problem of a spherical nanoparticle embedded in a finite spherical elastic body and established that as the inclusion size is reduced to nanometers, the impact of the surface and interface stress effects becomes significant. The large surface-to-volume ratio yields a significant surface stress, which is simultaneously strengthened by the high curvature of the surface. Furthermore,

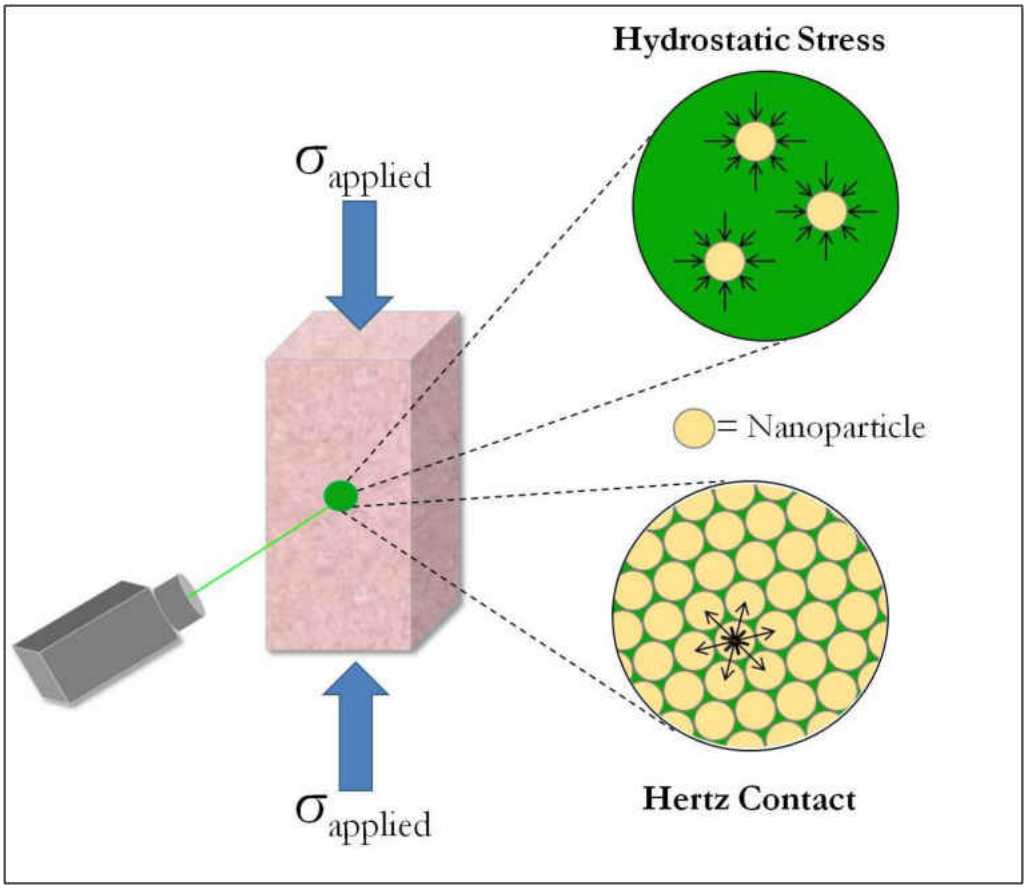

Figure 4.6: Schematic of possible load transfer mechanisms whereby quantitative data is captured by our piezospectroscopic measurements

the effect of the surface and interface elasticity strongly depends on the stiffness of the nanoparticle as well as the magnitude of the external loading. The sub-micron behavior at the nanoparticle-matrix interface is key to understanding and improving the strength and toughness of these adhesives and nanocomposites in general. At low loads and/or low volume fractions, the particles are expected to be under hydrostatic stress conditions as shown in Figure 4.6. At higher loads and/or high volume fractions, hertzian

theory defines the stress due to interparticle contact [19] which becomes the dominant mechanism.

Assuming a hydrostatic condition, the known PS relationship for a polycrystalline material is given as [23]:

$$\Delta v_{poly} = \Pi_H \sigma_H \tag{4.2}$$

where Π_H is 7.59 cm^{-1}/GPa for the R1 line and $7.615 cm^{-1}/GPa$ for the R2 line.

The PS relationship for our nanocomposites earlier presented in Chapter 2 as Equation 2.12 is repeated here:

$$\Delta \nu_{NC} = \Pi_{NC} \sigma_{applied} \tag{4.3}$$

where $\Delta \nu_{NC}$ is the frequency shift of the alumina R-lines, Π is the PS coefficient, and $\sigma_{applied}$ is the external stress applied to the nanocomposite.

The above relates the observed peak shifts with the applied load. Since the photostimulated luminescence shift from the nanocomposite is directly related to the average stress within the large number of nanoparticles under hydrostatic stress, we can equate the two peakshifts as follows:

$$\Delta \nu_{NC} = \Delta v_{poly} \tag{4.4}$$

Table 4.4: Hydrostatic stress transfer ratio to nanoparticles for different volume fractions

Specimen Type (%)	$\frac{\sigma_H}{\sigma_{applied}}$ (R1)	$\frac{\sigma_H}{\sigma_{applied}}$ (R2)
5	0.42	0.34
25	0.48	0.45
38	0.74	0.68

From this, we can therefore relate the hydrostatic stress on the particles with the applied stress as follows:

$$\frac{\sigma_H}{\sigma_{applied}} = \frac{\Pi_{NC}}{\Pi_H} \tag{4.5}$$

Using our measured values for the PS coefficients of R1 and R2 for each of the different volume fractions coulpled with Equation 4.5, we can infer the ratio of the externally applied stress that is transferred to the nanoparticles as being $\frac{\sigma_H}{\sigma_{applied}}$. These calculated values are presented in Table 4.4.

The results show a trend of increasing load transfer with higher volume fractions which is consistent with the improved mechanical properties of similar nanocomposites that have been tested for mechanical strength. The results from the R1 and R2 peaks correspond in this trend but differ quantitatively with R1 showing a higher load transfer than R2. A possible explanation for this variation, based on our measurements of PS coefficients, is that the R1 line is more sensitive to frequency shift with stress. This relationship

between particle content and PS coefficient values, therefore, has the potential to provide critical experimental data on the load transfer mechanisms in these nanocomposites and a calibration for optimized mechanical properties with the addition of fillers using the PS behavior of nanoparticles as stress indicators. Here, variations in the particle size, morphology, and the effects of nanoparticle surface modification (silane treatments) [60] on the effectiveness of load transfer can be assessed experimentally and compared with theoretical studies.

In summary, our PS results for the alumina nanocomposites are consistent with theoretical and analytical studies and provide a direct empirical relationship between the applied stress given to the nanocomposite and the spectral peak positions, therefore enabling the stress-sensing capability in these materials.

4.2.3 Discussion on Residual Stresses in Manufactured Samples

Residual stresses are produced in polycrystalline alumina upon cooling due to a difference in the thermal expansion coefficients with respect to the crystallographic axes [31, 33, 29]. Residual stresses are complex to analyze and the full details of the stress distribution are usually unknown, allowing for only average values for the residual stresses within polycrystalline alumina to be obtained. For epoxy composites cured at high temperatures (as the ones used here), substantial thermoelastic residual stresses are also created by a mismatch in the thermal expansion coefficients between the two differing materials. We

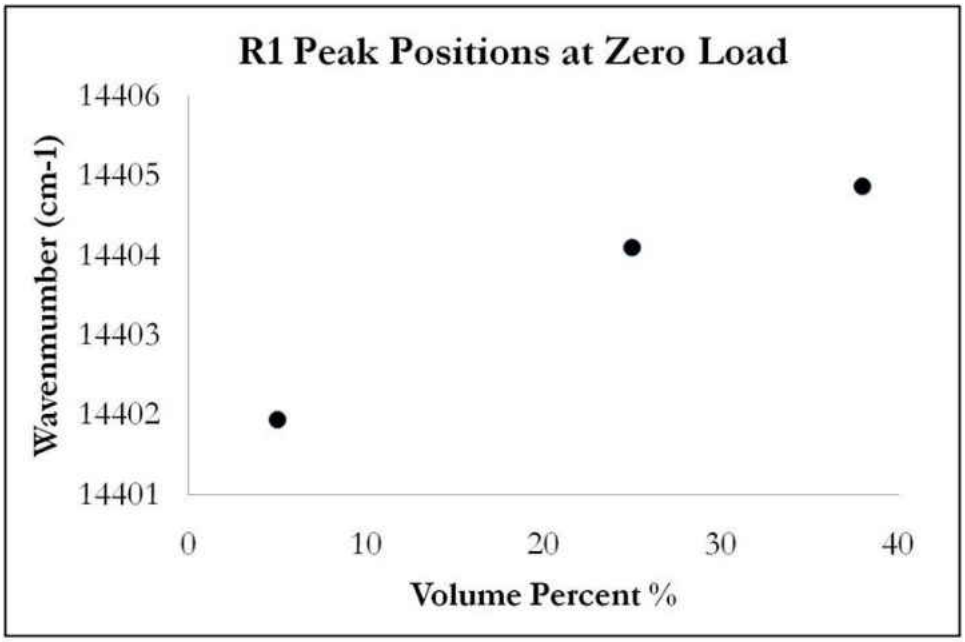

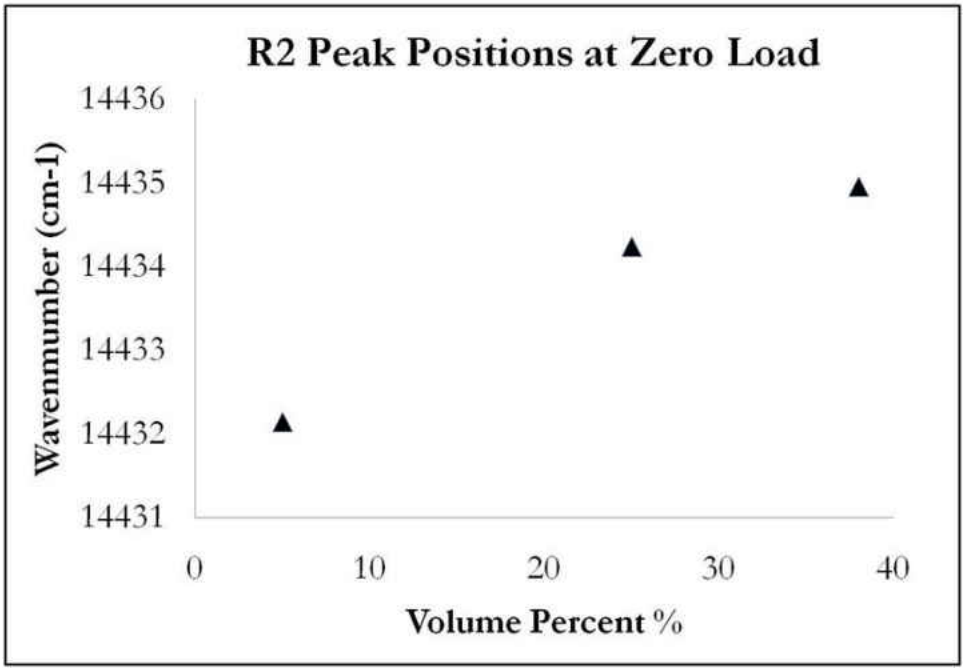

Figure 4.7: R-line peak positions at zero load; indication of residual stress

present here, the results that relate the residual stresses found in the alumina nanocomposite to alumina volume. Figure 4.7 shows the relationship between alumina particle

percentage to R-line peak positions in the absence of an external load. A trend is observed, suggesting that as the volume fraction of alumina increases, the initial peak position value tends toward a higher wavenumber, indicating an increased magnitude of residual stress.

4.3 Thermal Experiments

Previous work on ruby has indicated that the peak positions of the R-lines tend to shift toward smaller wavenumbers as temperature is increased [36, 43]. Calibration of peak shifts with stress to obtain the PS coefficients assumes temperature variations in the sample during the calibration process do not have a significant effect on the peak positions. This was verified for polycrystalline alumina by He and Clarke [23]. In this work, a temperature calibration was performed on each volume fraction material to establish quantitatively the temperature effects on the peak positions for the nanocomposites.

Figure 4.8: Experimental setup for the temperature studies

Table 4.5: R-line coefficients comparison (magnitude) with temperature.

Specimen Type (Volume Percent)	R1 Temp. Coefficient (α) $cm^{-1}/^oC$	R2 Temp. Coefficient (α) $cm^{-1}/^oC$
5	0.098	0.112
25	0.127	0.125
38	0.118	0.125

The temperature experiments were performed at the Argonne National Laboratory's Center of Nanoscale Materials. A Renishaw® Raman system accomodated a Linkam® thermal stage with a silver, liquid nitrogen-cooled sample holder. Each material was subjected to a temperature range of -25°C to +70°C with readings taken at 5 degree intervals. Figures 4.9, 4.10, and 4.11 show the linear relationship between the frequency shift of the R-lines and temperature.

Table 4.5 provides a quantitative R-line comparison of the PS coefficients with temperature. The temperature coefficient, (α), for each curve is much smaller than the determined PS coefficient produced by the stress-induced shifts. Therefore, the effects of temperature can be deemed as negligible and the calibrated shifts are assumed to result purely from the applied stress.

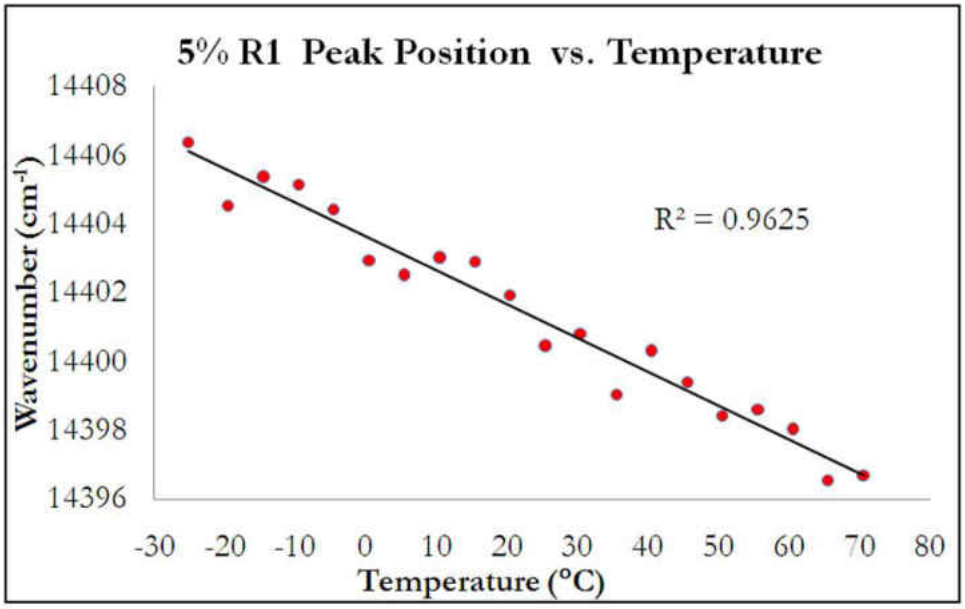

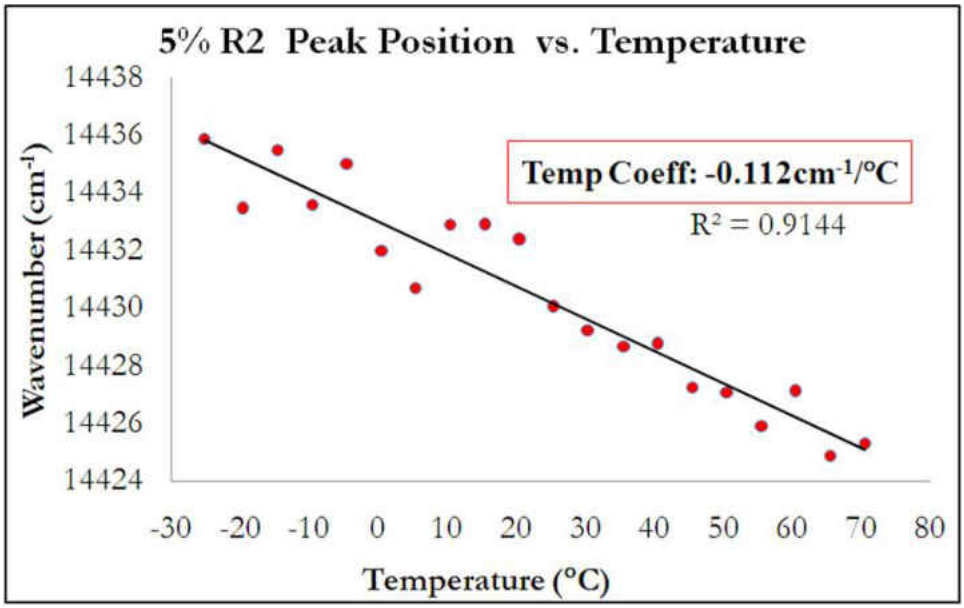

Figure 4.9: R1 and R2 Temperature Results for 5% volume fraction nanocomposite

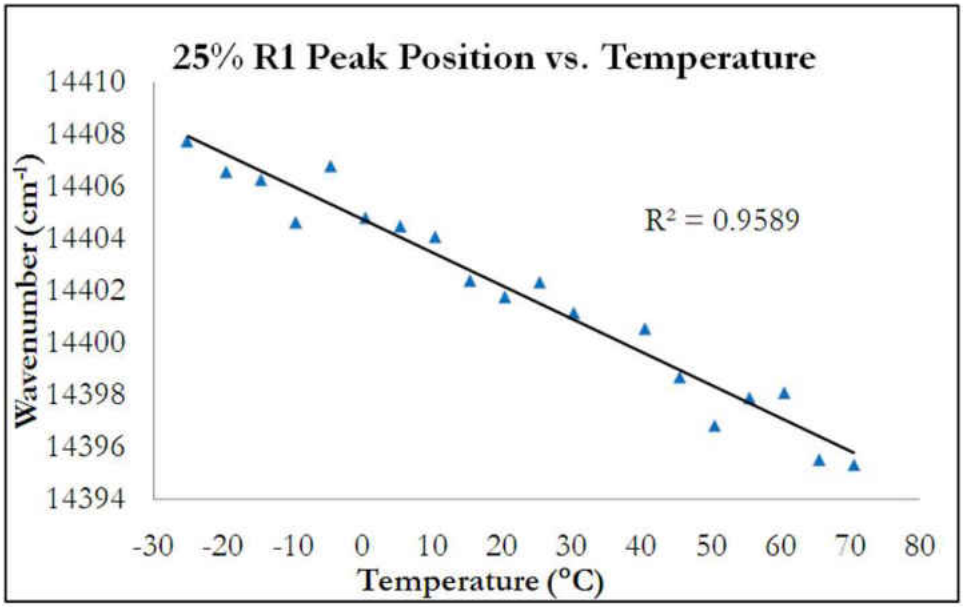

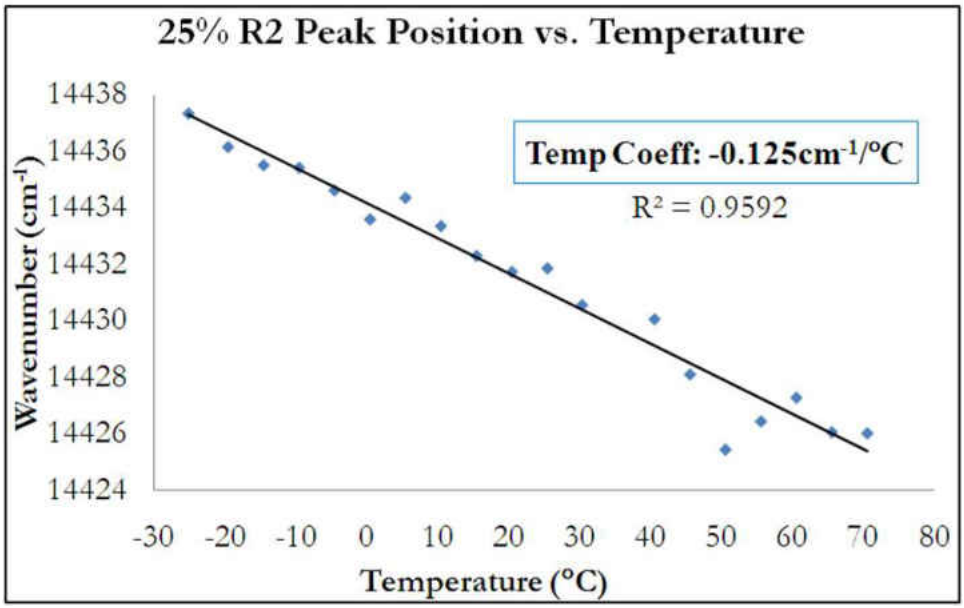

Figure 4.10: R1 and R2 Temperature Results for 25% volume fraction nanocomposite

4.4 Error Analysis

To ensure the validity of the photo-luminscence data collected during the in-situ compression tests, an analysis of the measurement error of the Raman spectrometer was

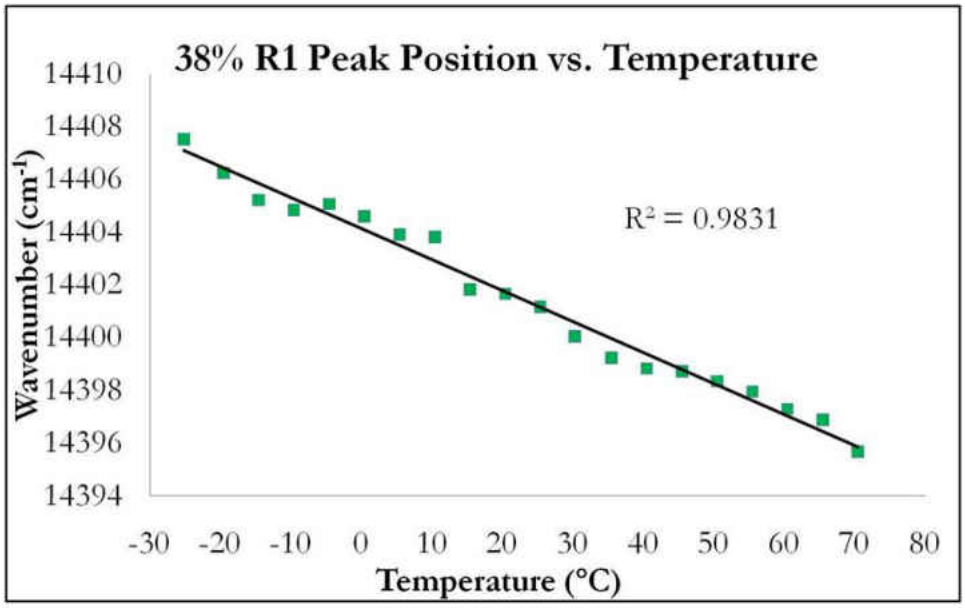

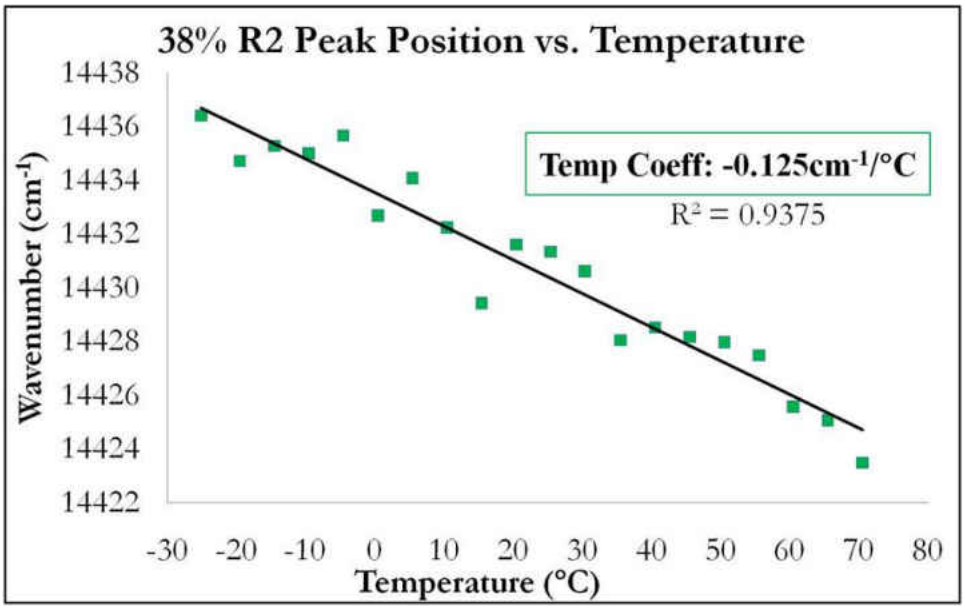

Figure 4.11: R1 and R2 Temperature Results for 38% volume fraction nanocomposite

performed using polycrystalline alumina. Fifty consecutive R-line spectrums were taken from one static point in the center of the polycrystalline specimen under load-free conditions. The data from each spectral collection was post-processed using the previously

described deconvolution method from Chapter 2 to obtain accurate R-line peak positions. These values, which describe the average variation between each measurement, were compared in order to determine the standard deviation, as shown in Figure 4.12. The standard deviations (1σ) were determined as 0.0086 and 0.0176 for the R1 and R2 lines, respectively. Comparison to the PS coefficients for the nanocomposites indicate that the error values contributed by the Raman spectrometer and deconvolution process are insignificant.

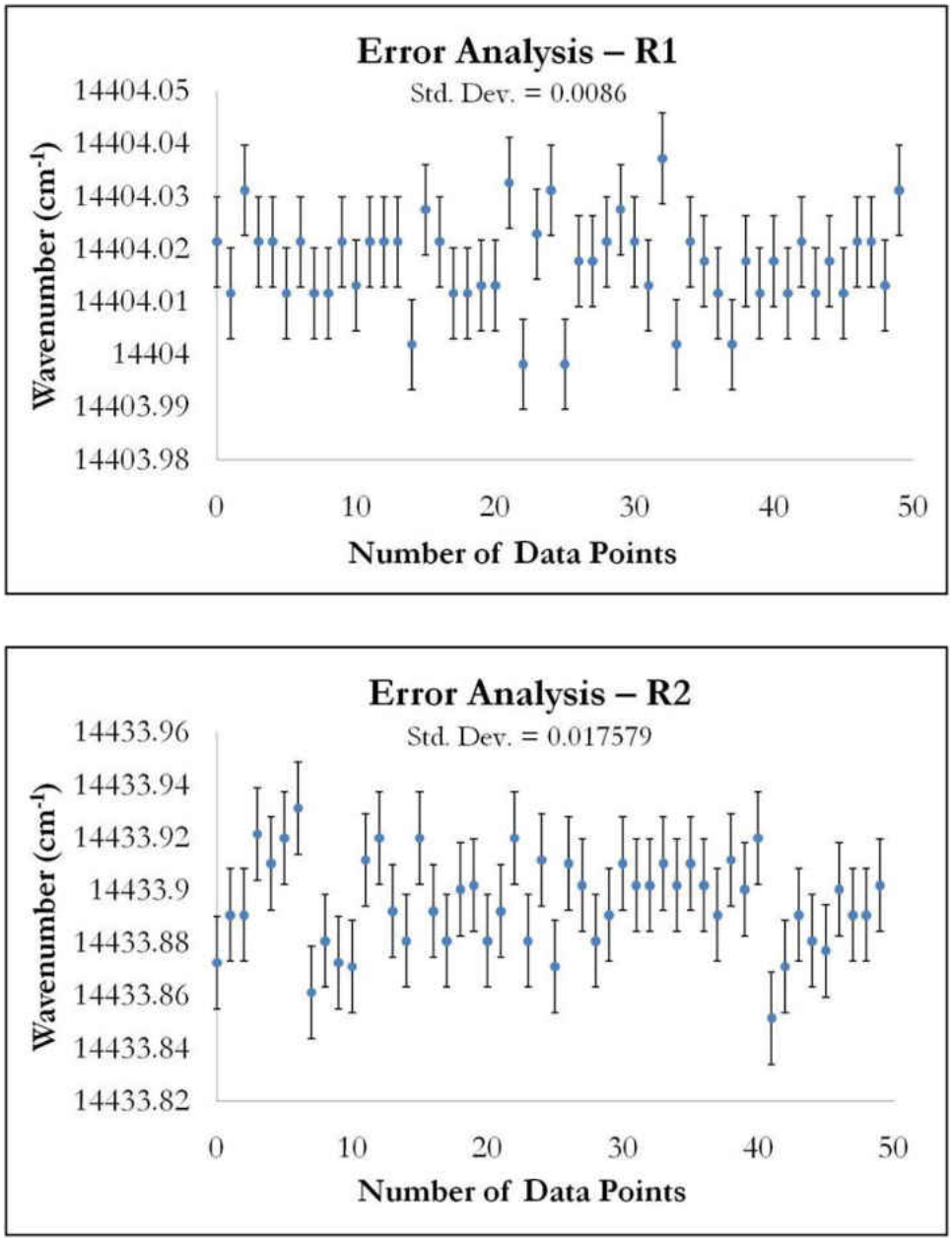

Figure 4.12: Standard deviation of PL data collected from polycrystalline alumina

CHAPTER 5
APPLICATION: SINGLE LAP SHEAR ADHESIVE TEST

5.1 Objectives

As technology advances, the need for non-invasive techniques to evaluate the integrity of aerospace structures increases. In Chapter 4, a calibration was designed using alumina-epoxy nanocomposites to provide a relationship between particle quantity and stress. An application is presented here, involving the creation of stress-sensing adhesives. By embedding epoxy adhesives with the previously studied alumina nanoparticles, the stress experienced by the material during a single lap-shear design configuration was determined. Using the spectral characteristic mapping technique presented in Chapter 3, real-time monitoring of stress prior to adhesive failure was possible by comparing the stress distributions throughout the sample surface as load increased. For future applications, the stress versus particle quantity calibrations created from the nanocomposite work may be used to determine appropriate volume fractions of alumina to achieve high mechanical properties with sufficient PS results.

5.2 Current Methods in Adhesive Integrity Testing

Using adhesives in the operational field requires extensive testing to assess the material's integrity and durability. Some of the currently used mechanical tests applied to adhe-

sives for the determination of mechanical properties include: lap shear tests (single and double), climbing drum peel tests, and tests to determine fracture toughness. Lap-shear configurations are designed such that an adhesive is bonded to substrates and then failed in tension under in-plane shear stress [21, 24, 61]. The two main types of lap-shear design are the single lap-shear and double lap-shear, both of which are capable of providing the lap-shear strength, which is determined by relating the maximum stress at the point of specimen failure. The peel strength of an adhesive can be determined by creating and testing cylindrical drum peel samples. The drum is rotated upward during the testing and the peel strength is determined by averaging out the energy required to pull the drum steadily and dividing this value by the specimen width. To determine the fracture toughness of adhesives, current techniques being used include the double cantilever beam (DCB) method, and the End-Notch Flexure (ENF) test. The DCB method is typically used to determine Mode I (opening mode) interlaminar fracture toughness by pre-cracking and pulling the specimen apart in tension. Using the ENF test design, a shear fracture is typically created in the specimen, allowing for the the Mode II (sliding, or shear) fracture toughness to be established. Lastly, the thick-adherend tensile-shear test is generally used as a test method to experimentally determine such material properties as the static and dynamic shear modulus, shear strength, and elongation at failure, under shear loading [26]. All of the above techniques used to determine the integrity of an adhesive rely on the deformation or failure of the specimen. The method proposed here using the PS technique offers a non-destructive, non-contact method for determin-

ing the stress distribution of the adhesive during tensile loading. During the real-time monitoring of the adhesive with applied stress, regions that experience the most stress can be evaluated to determine the main cause of specimen failure.

5.3 Single Lap-Shear Test Experiment

The single lap-shear design was chosen for simplicity in the representation of aerospace structural joints. ASTM Standard D5868 was followed as it is designed for determining the bonding characteristics of adhesives joined to both fiber reinforced plastics and metals. Two specimens, each 0.0254 m x 0.1016 m x 0.005 m (1 in x 4 in x 0.5 mm) were joined together with an adhesive infused with 13% volume α-alumina nanoparticles. Preceding research indicated an upper limit concentration of filler particles added to a polymer matrix for optimal mechanical properties ranged from 10% by weight [3] to 43% by volume [44]. Coupling these results with the quantity of photo-luminescent particles required to obtain sufficient PS measurements, led to the choice of 13% α-alumina by volume for the specimens in this test. The proper amounts of filler particles and epoxy/curing agent were measured and then hand-mixed for approximately 15 minutes. The adhesive overlap was 0.0254 m x 0.0254 m (1 in x 1 in) to ensure that failure would occur in the adhesive and not the substrate. The specimen was allowed to cure at room temperature in an arrangement such that the substrates remained parallel to each other during curing. The overall lap-shear configuration is shown schematically in Figure 5.1.

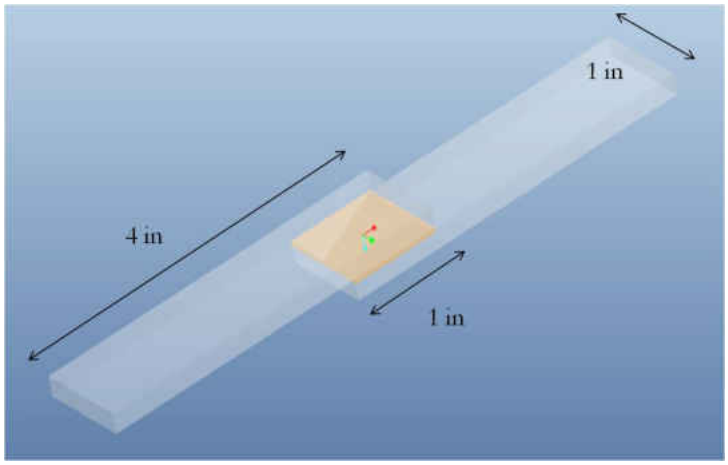

Figure 5.1: Single lap-shear configurations per ASTM D5868

The exact failure behavior of the α-alumina-embedded adhesive configuration tested here is not readily available in the literature. To ensure sufficient PS data was collected, small incremental tensile loads of 0.18 kN were applied at a rate of 13 mm/min (0.5 in/min) per to ASTM Standard D5868, until failure. Additionally, rubber shims were used to prevent the fiberglass from prematurely failing or slipping.

At every 50 MPa (0.18 kN) load, the experiment was held and photo-luminescent data from the modifier within the adhesive was collected in the form of a spectral surface map. The laser was focused using the intensity of the R-lines as a calibration tool. Similar to the compression tests on the nanocomposites, the optimal focal distance was reserved for all data collection points during the entire experiment. There were a total of 36 data collection points; 6 in the x-direction and 6 in the y-direction. The origin of the fiber optic probe was initially set in the upper-left-hand corner of the adhesive to begin each

surface map. A snake scan pattern, as shown in Figure 5.2, was automated by the x, y, z stage to collect independent photo-luminescent measurements at each of the 36 points.

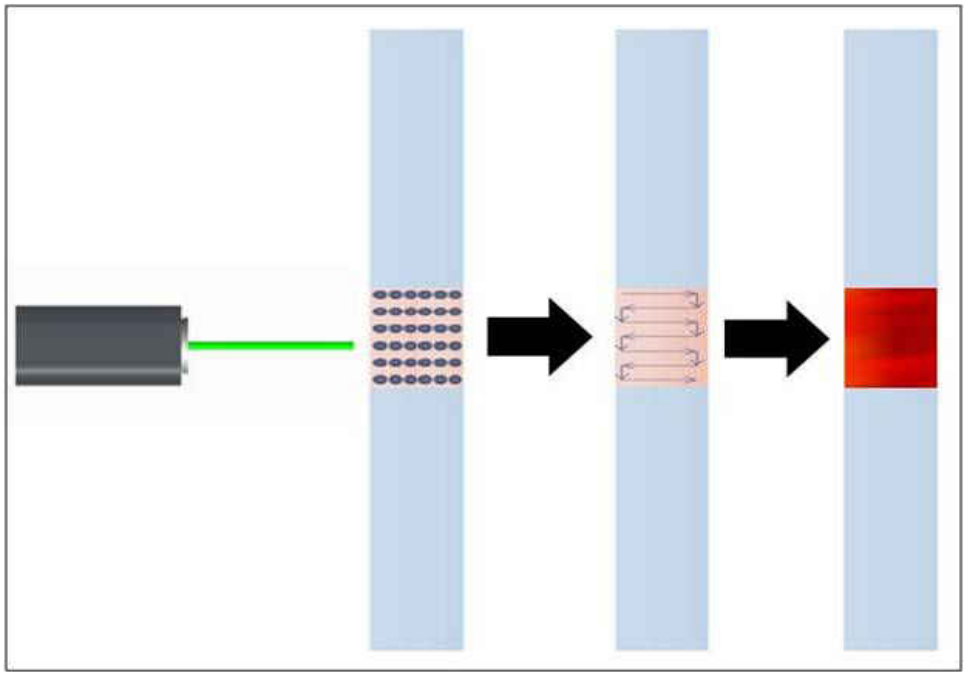

Figure 5.2: PSLS data collection pattern for an adhesive during tensile loading

5.4 Results and Discussion

Experiments to ensure that the fiberglass chosen had sufficient optical transparency were conducted prior to the tensile tests. Spectral data through the fiberglass from polycrystalline alumina and the epoxy-alumina composites consisting of various volume fractions of filler material were obtained and compared to measurements taken from the composites without the fiberglass. The results are shown in Figure 5.3 which clearly indicate sharp and distinct R-lines through the fiberglass, even for the 5% alumina volume frac-

tion composite. A small, consistent decrease in intensity was witnessed for all volume fraction specimens. This trend may be explained through the reduction in transmissibility of the laser through the fiberglass coupled with the difficulty in focusing the laser directly on the alumina composite. While the transmissibility may have contributed to the small decrease in the intensity, it was not sufficient enough to affect obtaining clear and distinct R-lines. The results of these tests verified the capability of real-time monitoring of the adhesives through fiberglass substrates and provided a quantitative volume fraction range of alumina that would successfully allow for substantial R-line peaks to be obtained.

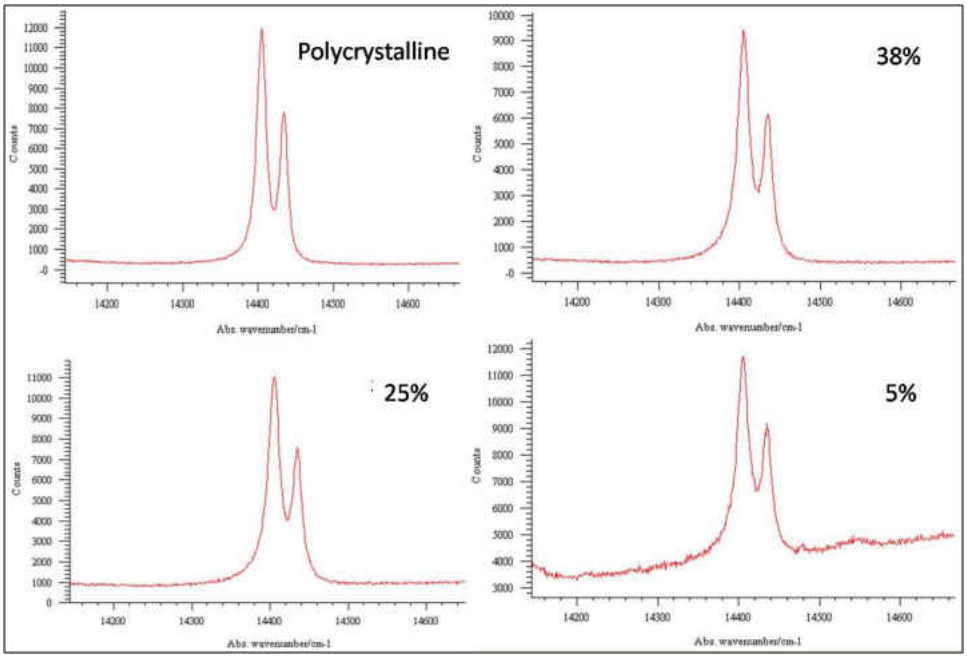

Figure 5.3: R-lines collected through fiberglass substrates from 4 alumina specimens.

Spectral characteristic maps comparing R1 peak positions were generated for three tensile loads of 0 kN, 0.6 kN, and 1.2 kN, corresponding to the reference load, inter-

mediate load, and maximum load, respectively. The map obtained from the unloaded lap-shear specimen contains an assortment of information regarding the adhesive prior to the loading tests. For a material experiencing a uniform state of stress, a corresponding homogenous and unvarying contour map is expected. Hence, if no external load is applied, all peak position values should be approximately equal. As seen in Figure 5.4, there is a clear deviation in the range of the R1 line peak positions prior to loading, which indicates pre-existing and fluctuating residual stresses on the α-alumina particles prior to the lap-shear tests. Possible explanations for the deviations in the unstressed R1 peak positions are uneven adhesive curing, and non-homogeneous particle dispersion. The focus of this work, however, was to evaluate whether the change in stresses within an adhesive can be monitored or observed non-destructively using the peak positions of the R-lines. Comparison of specific regions between the reference and loaded maps verify the capability of the proposed method in detecting the change in stresses of the R1 lines due to applied loading.

The ability to obtain spectral information from an entire sample surface has the potential to aide in the development of adhesives with optimal mechanical properties. Using photo-luminescent particles as polymer modifiers not only strengthens the material, but also provides a non-destructive means to observe the stress distribution within the adhesives when loaded up to failure. The method has the potential to provide high spatial resolution measurements and resolution can be adjusted to fit the dimensions of various samples. The combination of a fiber optic probe and Raman spectrometer

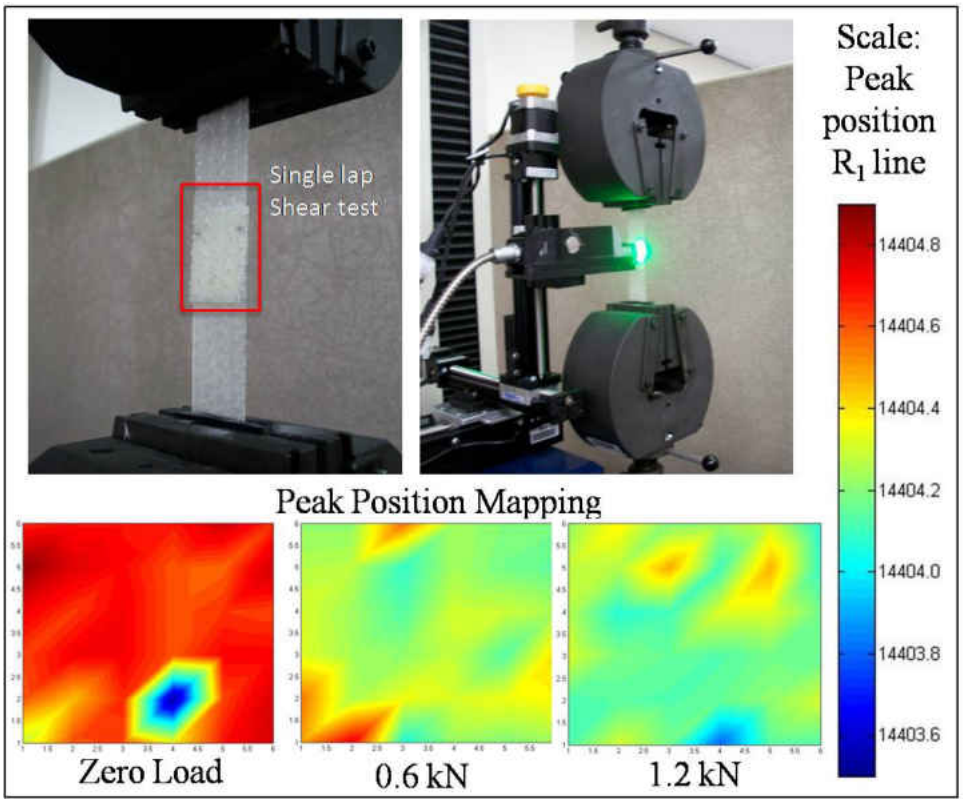

Figure 5.4: Stress distribution with respect to applied load. Peak positions of the R1 line throughout the adhesive are compared via a contour map.

has the capability of producing a laser spot size of about 1-2 microns, comparable to a microscope/spectrometer system configuration [11]. In addition, particle dispersion can be established over the reference material to assess homogeneity in manufacturing. Coupled with SEM and/or TEM imaging techniques, a complete evaluation of particle distribution can be confirmed.

CHAPTER 6
CONCLUSIONS

6.1 Summary of Results

The motivation of this research initiated from the need to invent a non-destructive means to assess the integrity of structures. Current methods used for this purpose are invasive and are deficient in the ability to quantitatively determine the stresses with a material prior to failure. Additionally, these methods are also incapable of high spatial measurements and also cannot assess load transfer mechanisms that are crucial in the development of optimized polymer-based materials. As such, the primary focus of this work was to design and create a novel approach with the ability to non-destructively evaluate real-time stress distributions prior to material failure. This was achieved by using the method of piezospectroscopy on embedded photo-luminescent α-alumina nanoparticles within a polymer matrix in order to determine the relationship between applied stress and the frequency shift of the characteristic R-lines produced from the alumina. From this work, we have determined quantitative values for PS coefficients that calibrate the stress-sensing property of the alumina-epoxy nanocomposites. Six coefficients were obtained for each of the volume fraction specimens, representing the behavior of both the R1 and R2 peaks with stress. With these coefficients we have successfully designed a method for enabling the implementation of stress-sensing polymer-based materials that can be used for structural integrity monitoring. By applying this technique to an adhesive in a single lap-shear configuration, we have demonstrated the capability of discerning peak shifts of

the R-lines with high spatial resolution, which can be used to evaluate stress distributions. Laboratory-based implementation of this technique for real-time stress monitoring provides the potential for formulating adhesives with enhanced mechanical properties.

Additionally, this work will help in improving fabrication and manufacturing standards of nanocomposites through quality control. By mapping the intensity characteristics of the alumina nanocomposites and relating this to particle dispersion we have effectively established a novel approach to assess the homogeneity of particle dispersion within a polymer-based nanocomposite. Quantitative comparison of the intensities between volume fraction specimens allowed us to determine a relationship between filler material quantity with the spectral property. This provides a measurement tool that enables verification of the particle volume fraction within manufactured nanocomposites.

The significant contribution of this work lies in the capability of numerically assessing load transfer to the particles within a nanocomposite, which can be achieved through piezospectroscopic measurements. The relationship between particle content and PS coefficient values presented in this work has the potential to provide critical experimental data on the load transfer mechanisms in these nanocomposites. With our results and findings, a calibration for optimized mechanical properties with the addition of fillers using the piezospectroscopic behavior of alumina nanoparticles as stress indicators can be obtained.

6.2 Future Work

The piezospectroscopic calibration has provided an overall relationship between the external stress and the emission peak positions of the nanoparticles when excited with a laser. While the calibrated coefficients to the external stress will provide the basis for a spectral characteristic mapping system, data on the actual stresses experienced by the nanoparticles will become experimentally available by our study. This will lead to a fundamental understanding of the interface elasticity and load transfer between the epoxy and nanoparticles. Development of the testing method for the stress sensing material, forms an important motivation for laboratory-based efforts to understand how adhesive performance can be improved through filler particles. The stress sensing capabilities of alumina nanoparticles will provide experimental data relevant to uncover and understand nanoparticle behavior. The piezospectroscopic nature of these particles make them ideal to facilitate experimental discoveries related to high interface stresses and enable insight on the mechanical strengthening mechanisms at the nanoscale. The ability to perform piezospectroscopic studies on a single alumina nanoparticle has recently been made possible with advances in combined AFM-Raman instrumentation. Potentially, stress mapping on an individual nanoparticle in epoxy under load is achievable. With specific focus on experimental stresses measured at the interface, individual particle piezospectroscopic behavior can be linked to microprobe based studies through volume averaging of particle data while assessing effects of particle morphology, size, distribution, and filler

content. This adds a new dimension to nanoparticle research, expanding the capabilities through experimental techniques.

LIST OF REFERENCES

[1] J. D. Barnett, S. Block, and G. J. Piermarini. An optical fluorescence system for quantitative pressure measurement in the diamond anvil cell. *The Review of Scientific Instruments*, 44:1–9, 1973.

[2] R. Bossi, K. Housen, and C. Walters. Laser bond inspection device for composites: Has the holy grail been found ? Technical report, NonDestructive Testing Information Analysis Center Newsletter, 2005.

[3] D. Clarke, R. Christensen, and V. Tolpygo. Evolution of oxidation stresses in zirconia thermal barrier coated superalloy leading to spalling failure. *Surface Coatings and Technology*, 94-95:89–93, 1997.

[4] D. Clarke and D. Gardiner. Recent advances in piezospectroscopy. *International Journal of Materials Research*, 98:8, 2007.

[5] W. Crossley and E. Williams. A study of adaptive penalty functions for constrained genetic algorithm-based optimization. In *AIAA meeting papers*, 1997.

[6] D. H. C. Dai Gil Lee, Jin Kook Kim. Effects of adhesive fillers on the strength of tubular single lap adhesive joints. *Journal of Adhesion Science Techonology*, 13:1343–1360, 1999.

[7] B. Derby. Ceramic nanocomposites: mechanical properties. *Current Opinion in Solid State and Materials Science*, 3:490–495, 1998.

[8] B. Ehrhart, B. Valeske, C.-E. Muller, and C. Bockenheimer. Methods for the quality assessment of adhesive bonded cfrp structures - a resume. In *2nd International Symposium on NDT in Aerospace 2010*, 2010.

[9] J. Eshelby. The determmination of the elastic field of an ellipsoidal inclusion and related problems. *Proceedings of the Royal Society of London. Series A, Mathematical and Physical Sciences*, 241:376–396, 1957.

[10] V. Evora, N. Jain, and A. Shukla. Stress intensity factors and crack velocity relationships for polyester/tio2 nanocomposite. *Experimental Mechanics*, 45:153–159, 2005.

[11] E. Feher and M. Sturge. Effect of stress on the trigonal splittings of d^3 ions in sapphire. *Physical Review*, 172:244–249, 1968.

[12] R. A. Forman, G. J. Piermarini, J. D. Barnett, and S. Block. Pressure measurement made by the utilization of ruby sharp-line luminescence. *Science*, 176:284–285, 1972.

[13] G. Freihofer, L. Poliah, K. Walker, A. Medina, and S. Raghavan. Optical stress probe: In situ stress mapping with raman and photo-stimulated luminescence spectroscopy. *Journal of Instrumentation*, 5:P12003, 2010.

[14] D. J. Gardiner, M. Bowden, S. Margueron, and D.R. Use of polarization in imaging the residual stress in polycrystalline alumina films. *Acta Materia*, 55:3431–3436, 2007.

[15] M. Gell, S. Sridharan, and M. Wen. Photoluminescence piezospectroscopy a multil purpose quality control and ndi technique for thermal barrier coatings. *International Journal of Applied Ceramics Technology*, 1(4):316–329, October 2004.

[16] E. N. Gilbert, B. S. Hayes, and J. C. Seferis. Nano-alumina modified epoxy based film adhesives. *Polymer Engineering and Science*, 43 No. 5:1096–1104, May 2003.

[17] H. Gleiter. Nanostructured materials: basic concepts and microstructure. *Acta Mater*, 48:1–29, 2000.

[18] L. Grabner. Spectroscopic technique for the measurement of residual stress in sintered al2o3. *Journal of Applied Physics*, 49(5):580–583, 1978. .pdf ok.

[19] V. G. Gryaznov, M. Y. Tanakov, and L. I. Trusov. Review: Plasticity and mass-transfer in contacting nanoparticles. *Journal of materials science*, 27:4829–4841, 1992.

[20] M. E. Gurtin, J. ller, and F. Larche. A general theory of curved deformable interfaces in solids at equilibrium. *PHILOSOPHICAL MAGAZINE A*, 78 No. 5:1093–1109, 1998.

[21] L. J. Hart-Smith. Adhesive bonded single-lap joints. Technical report, NASA, 1973.

[22] He and Clarke. Polarization dependence of the cr^{3+} r line fluorescence from sapphire and its application to crystal orientation and piezospectroscopic measurement. *Journal of the American Ceramic Society*, 80(1):69–78, June 1997.

[23] J. He and D. R. Clarke. Determination of the piezospectroscopic coefficients for chromium doped sapphire. *Journal of American Ceramic Society*, 78(5):1347–1353, 1995.

[24] A. Higgins. Adhesive bonding of aircraft structures. *International Journal of Adhesion & Adhesives*, 20:367–376, 2000.

[25] T. Ida, M. Ando, and H. Toraya. Extended pseudo voigt function for approximating the voigt profile. *Journal of Applied Crystallography*, 33:1311–1316, July 2000.

[26] C. A. Jose M. Arenas, Julian J.Narbon. Optimum adhesive thickness in structural adhesives joints using statistical techniques based on weibull distribution. *International Journal of Adhesion & Adhesives*, 30:160–165, 2010.

[27] A. A. Kaplyanskii and A. K. Przhevuskii. The piezospectroscopic effect in ruby crystals. *Soviet Physics - Dokaldy*, 7(1):313–316, July 1962.

[28] J. F. Kielkopf. New approximation to the voigt function with applications to spectral-line profile analysis. *Journal of the optical society of america*, 63:987–995, 1973.

[29] M. Kronberg. Plastic deformation of single crystals of sapphire : Basal slip and twinning. *Acta Metallurgica*, 5:507–524, september 1957.

[30] M. Y. Lee, S. K. Ahn, and S. T. Montgomery. Statistical analysis of compositional factors affecting the compressive strength of alumina-loaded epoxy. Technical report, SANDIA National Laboratory, February 2006.

[31] Q. Ma and D. R. Clarke. Stress measurement in single-crystal and polycrystalline ceramics using their optical fluorescence. *Journal of the American Ceramic Society*, 76(6):1433–1440, 1993.

[32] Q. Ma and D. R. Clarke. Piezospectroscopic determination of residual stresses in polycrystalline alumina. *Journal of American Ceramic Society*, 77:298–302, 1994.

[33] Q. Ma, W. Pompe, J. French, and D. Clarke. Residual stresses in $al_2o_3 - zro_2$ composites: A test of stochastic stress models. *Acta Metallurgica et Materialia*, 42:1673–1681, 1994.

[34] S. Margueron and D. R. Cla. Effect of polarization and uniaxial stress on the r-line luminescence of single crystal sapphire. *Journal of Applied Physics*, 101:094902, 2007.

[35] S. Margueron and D. Clarke. The use of polarization in the piezospectroscopic determination of the residual stresses in polycrystalline alumina ?lms. *Acta Materialia*, 54:5551–5557, 2006.

[36] D. E. McCumber and M. D. Sturge. Linewidth and temperature shift of the r lines in ruby. *Journal of Applied Physics*, 34(6):1682–1684, January 1963.

[37] L. M. McGrath, R. S. Parnas, S. H. King, J. L. Schroeder, D. A. Fischer, and J. L. Lenhart. Investigation of the thermal, mechanical, and fracture propertiesof alumina-epoxy composites. *Polymer*, 49:999–1014, 2008.

[38] C. Mi and D. Kouris. Nanoparticles and the influence of interface elasticity. *Theoret. Appl. Mech.*, 35 No. 1-3:267286, 2008.

[39] C. MI and D. A. KOURIS. The role of interface stress for nanoparticles embedded in films. *Journal of Solid Mechanics and Materials Engineering*, 1 No. 10:1219–1230, 2007.

[40] J. C. F. Millett, D. Deas, N. K. Bourne, and S. T. Montgomery. The deviatoric response of an alumina filled epoxy composite during shock loading. *Journal of Applied Physics*, 102:063518–1–6, 2007.

[41] V. Mittal, editor. *Optimization of Polymer Nanocomposite Properties*. WILEY-VCH, 2010.

[42] S. E. Molis and D. R. Clarke. Measurement of stresses using fluorescence in an optical microprobe: Stresses around indentations in a chromium-doped sapphire. *Journal of Electronic Structure of Ceramics*, 73(11):3189 –3194, 1990.

[43] R. Munro, G. Piermarini, S.Block, and W. Holzapfel. Model line shape analysis for the ruby r lines used for pressure measurement. *Journal of Applied Physics*, 57:165–169, 1985.

[44] D. E. Munson and K. Schuler. Steady wave analysis of wave propagation in laminates and mechanical mixtures. *Journal of Composite Materials*, 5:286–304, 1971.

[45] N. Muraki, N. Matoba, T. Hirano, and M. Yoshikawa. Determination of thermal stress distribution in a model microelectronic device encapsulated with alumina filled epoxy resin using fluorescence spectroscopy. *Polymer*, 43:1277–1285, 2002.

[46] J. Nychka and D. Clarke. Damage quantification in TBCs by photo-stimulated luminescence spectroscopy. *Surface Coatings and Technology*, 146-147:110–116, 2001.

[47] E. M. Petrie. Adhesives for the assembly of aircraft structures and components. *Metal Finishing*, pages 26–31, February 2008.

[48] A. P. Petrova and N. F. Lukina. Adhesive technologies in aircraft construction. *Polymer Science, Series D. Glues and Sealing Materials*, 1:83–90, 2008.

[49] V. Pryamitsyn and V. Ganesan. Origins of linear viscoelastic behavior of polymer: Nanoparticle composites. *Macromolecules*, 39:844856, 2006.

[50] M. U. A. R. E. Setchell and S. T. Montgomery. Compositional effects on the shock-compression response of alumina-filled epoxy. *Journal of Applied Physics*, 101:083527, 2007.

[51] S. Raghavan and P. Imbrie. The development of photo-stimulated luminescence spectroscopy for 3d stress measurements in the thermally grown oxide layer of thermal barrier coatings. In *Proceedings of the Materials Science and Technology 2007 conference*, 2007.

[52] S. Raghavan, P. Imbrie, and W. A. Crossley. The spectral analysis of R lines and vibronic sidebands in the emission spectrum of ruby using genetic algorithms. *Applied Spectroscopy*, 62:759–765, 2008.

[53] S. Raghavan and P. K. Imbrie. Ex-situ stress measurements in polycrystalline ceramics using photo-stimulated luminescence spectroscopy and high-energy x-rays. *The American Ceramic Society*, 11 No. 11:1–7, 2009.

[54] A. Schawlow. Fine structure and properties of chromium fluorescence in aluminum and magnesium oxide. *Advances in Quantum Electronics*, 2:50–64, 1961. .pdf ok.

[55] A. Selcuk and A. Atkinson. Analysis of the Cr^{3+} luminescence spectra from thermally grown oxide in thermal barrier coatings. *Materials Science and Engineering A*, A335:147–156, 2002. .pdf ok.

[56] P. Sharma and S. Ganti. Size-dependent eshelbys tensor for embedded nano-inclusions incorporating surface/interface energies. *Journal of Applied Mechanics*, 71:663–671, 2004.

[57] R. Siegel, S. K. Chang, A. J. Stone, P. Ajayan, R. W. Doremus, and L. Schadler. Mechanical behavior of polymer and ceramic matrix composites. *Scripta Mater.*, 44:2061–2064, 2001.

[58] B. Song, W. Chen, S. Montgomery, and M. Forrestal. Mechanical response of an alumina-filled epoxy at various strain rates. *Journal of Composite Materials*, 43:1519–1536, 2009.

[59] S. Sridharan, L. Xie, E. H. Jordan, and M. Gell. Stress variation with thermal cycling in the thermally grown oxide of an eb-pvd thermal barrier coating. *Surface Coatings and Technology*, 179:286–296, 2004.

[60] M. Tanoglu, S. McKnight, G. Palmese, and J. G. Jr. Use of silane coupling agents to enhance the performance of adhesively bonded alumina to resin hybrid composites. *International Journal of Adhesion & Adhesives*, 18:431–434, 1998.

[61] J. Tomblin, W. Seneviratne, H. Kim, and J. Lee. Characterization of in-plane, shear-loaded adhesive lap joints experiments and analysis. Technical report, Department of Aerospace Engineering Wichita State University Wichita, KS 67260-0093 *School of Aeronautics and Astronautics Purdue University West Lafayette, IN 47907-1282, 2003.

[62] G. Wertheim, M. Butler, K. West, and D. Buchanan. Determination of the gaussian and lorentzian content of experimental line shapes. *Review of Scientific Instruments*, 45:1369–1371, 1974.

[63] B. Wetzel, F. Haupert, and M. Q. Zhang. Epoxy nanocomposites with high mechanical and tribological performance. *Composites Science and Technology*, 63:2055–2067, 2003.

[64] B. Wetzel, P. Rosso, F. Haupert, and K. Friedrich. Epoxy nanocomposites - fracture and toughening mechanisms. *Engineering Fracture Mechanics*, 73:2375–2398, 2006.

[65] E. Williams and W. Crossley. Empirically derived population size and mutation rate guidelines for a genetic algorithm with uniform crossover. In *Soft Computing in Engineering Design and Manufacturing*, 1998.

[66] A. Wright, C. Gonzalez, A. Jones, and S. Raghavan. Piezospectroscopic measurements on alumina epoxy composites. In *Proceedings of the 51st AIAA/ASME/ASCE/AHS/ASC Structures, Structural Dynamics and Materials Conference, Orlando, Florida*, 2010.

[67] A. L. Wright and S. Raghavan. Effects of stress on alumina nanocomposites using piezospectroscopy. In *Proceedings of the Society for the Advancement of Material and Process Engineering 2010 conference, Seattle, Washington*, 2010.

[68] D. Xie, J. Chung, A. Waas, K. Shahwan, J. Schroeder, R. Boeman, V. Kunk, and L. Klett. Failure analysis of adhesively bonded structures: from coupon level data to structural level predictions and verification. *International Journal of Fracture*, 134:231250, 2005.

[69] C. Yang and J. S. Tomblin. Investigation of adhesive behavior in aircraft applications. Technical report, Office of Aviation Research, September 2001.

[70] S. Zhao, L. S. Schadler, H. Hillborg, and T. Auletta. Improvements and mechanisms of fracture and fatigue properties of well-dispersed alumina/epoxy nanocomposites. *Composites Science and Technology*, 68:2976–2982, 2008.

[71] S. C. Zunjarrao and R. P. Singh. Characterization of the fracture behavior of epoxy reinforced with nanometer and micrometer sized aluminum particles. *Composites Science and Technology 66 (2006) 22962305*, 66:2296–2305, 2006.